General Disclaimer

One or more of the Following Statements may affect this Document

- This document has been reproduced from the best copy furnished by the organizational source. It is being released in the interest of making available as much information as possible.

- This document may contain data, which exceeds the sheet parameters. It was furnished in this condition by the organizational source and is the best copy available.

- This document may contain tone-on-tone or color graphs, charts and/or pictures, which have been reproduced in black and white.

- This document is paginated as submitted by the original source.

- Portions of this document are not fully legible due to the historical nature of some of the material. However, it is the best reproduction available from the original submission.

Produced by the NASA Center for Aerospace Information (CASI)

NAG 5-105

CLOUD/CLIMATE SENSITIVITY EXPERIMENTS

(NASA-CR-170096) CLOUD/CLIMATE SENSITIVITY EXPERIMENTS (California Univ.) 50 p HC A03/MF A01 CSCL 04B

N83-21709

Unclas

G3/47 03179

John O. Roads

Geoffrey K. Vallis

Lorraine Remer

MAR 1983
RECEIVED
NASA STI FACILITY
ACCESS DEPT.

Climate Research Group

Scripps Institution of Oceanography

University of California, San Diego, A-024

La Jolla, California 92093

ORIGINAL PAGE IS
OF POOR QUALITY

Invited paper presented at the fourth biennial Ewing Symposium, Lamont-Doherty Geological Observatory, October 25-27, 1982.

Abstract

A study of the relationships between large-scale cloud fields and large-scale circulation patterns is presented. The basic tool is a multi-level numerical model comprising conservation equations for temperature, water vapor and cloud water and appropriate parameterizations for evaporation, condensation, precipitation and radiative feedbacks. Incorporating an equation for cloud water in a large-scale model is somewhat novel and allows the formation and advection of clouds to be treated explicitly. The model is run on a two-dimensional, vertical-horizontal grid with constant winds. It is shown that cloud cover increases with decreased eddy vertical velocity, decreased horizontal advection, decreased atmospheric temperature, increased surface temperature, and decreased precipitation efficiency. The cloud field is found to be well correlated with the relative humidity field except at the highest levels. When radiative feedbacks are incorporated and the temperature increased by increasing CO_2 content, cloud amounts decrease at upper-levels or equivalently cloud top height falls. This reduces the temperature response, especially at upper levels, compared with an experiment in which cloud cover is fixed.

ORIGINAL PAGE IS
OF POOR QUALITY

PRECEDING PAGE BLANK NOT FILMED

ORIGINAL PAGE IS
OF POOR QUALITY

1. Introduction

The compensating features of the cloud greenhouse and the cloud albedo effects, allied to possible changes in cloud height, distribution, and characteristics complicate our understanding of the response of the climate to external stimuli, such as increased CO_2 levels. The problem is twofold. First it is necessary to understand the radiative effects of cloud cover. This has been discussed by Ohring and Clapp (1980), Cess and Ramanathan (1978), Schneider (1972) and many others. The second, and less well understood, problem lies in understanding the causes of cloud variability, or alternatively predicting cloud response in a given situation. Predicting cloud response does not simply involve predicting total cloud cover. For example, Schneider has demonstrated the importance of the cloud top height. If cloud top height increases then the effective emitting temperature decreases and the greenhouse effect is enhanced. On the other hand, if total cloud area is simply increased then it is likely that the albedo effect will outweigh the greenhouse effect (e.g., Hartmann and Short, 1980). However, Cess (1976) and Cess *et al* (1982) argue that the competing cloud effects may compensate each other very closely at all latitudes and seasons. Presumably, this does not mean that effects at individual longitudes will also be closely compensated (Shukla and Sud, 1981).

Much has been written about the physical characteristics affecting cloud formation and associated precipitation (for a comprehensive account see Ludlum, 1980). The task facing climatologists is not only to understand where and why clouds of various shapes, sizes and characteristics form but to parameterize this in terms of the large scale. Although simple parameterizations of cloud cover, such as setting it a function of relative humidity (first suggested by Smagorinsky, 1960; see also Slingo, 1980) or allowing cloud where condensation occurs, appear at first glance to give climatologically acceptable results in GCM's, high clouds are poorly treated and hence even qualitative uncertainty in the radiative feedbacks must arise. Furthermore, it seems that the parameterizations must be tuned to the particular GCM used, clearly an unsatisfactory procedure.

At the risk of oversimplifying cloud physics, let us assume that clouds occur primarily where parcels of air become supersaturated with respect to a plane surface. If the rate at which supersaturation occurs is sufficiently large to produce sufficiently large amounts of cloud water, then coalescence and

ORIGINAL PAGE IS
OF POOR QUALITY

accretion of various cloud drops produce still larger drops which eventually fall to the surface. Transport processes will extend clouds into regions (both space and time) where cloudwater evaporates. While the above notions are partially understood in specific cases, the associated large-scale processes that will produce regions of supersaturation and subsaturation are numerous and not well understood. A number of workers, including Manabe and Wetherald(1975), Roads(1978a), Schneider *et al*(1978), and Wetherald and Manabe(1980) have shown that middle tropospheric clouds tend to decrease with increasing temperature even though the intensity of the hydrologic cycle (precipitation and evaporation) increased. The explanation is that with a more intense hydrologic cycle, the vertical velocity variance tends to increase, resulting in more precipitation in regions of ascent and more drying in regions of descent. In regions of descent where cloud cover was already present or under conditions where horizontal advection of dry air is important, the drying effects have more effect on the cloud cover than the moistening effects and hence cloudiness decreases with increasing temperature.

There are certainly other factors influencing the cloud fields. Roads (1978b), for example, has shown that under certain conditions zonal mean cloud cover can be decreased by increasing the mean downward zonal velocity, by increasing the diabatic heating, by increasing the static stability and by decreasing the scaled evaporation, q_γ. Scaled evaporation is the ratio of the surface saturated humidity, q_s^*, to an atmosphere saturated humidity, q_a^*. If temperature alone increases, but lapse rate remains the same, the scale evaporation decreases, since $\partial/\partial T(q_\gamma) < 0$ for $T_s > T_a$.

In a GCM experiment, Wetherald and Manabe (1980) found that low level fractional cloud coverage actually increased with increasing temperature in high latitudes. (Similar results were also found by Potter *et al* (1981)). This occurred over a region in which surface albedo decreased rapidly, due to the poleward retreat of the surface ice sheet, causing surface temperatures to rise noticeably - a rise of 19K was found at latitude 80° in Wetherald and Manabe's model due to a 6% rise is solar constant. Atmospheric temperatures did not rise as rapidly, because of the moderating influences of cross-latitude heat exchange. Vallis (1982), Roads and Vallis (1982) explained this using relatively simple zonally averaged models. As the ice sheet retreated, the lower atmosphere (in high latitudes) was destabilized and an increase in scaled surface evaporation ensued which caused cloud cover to increase. In lower lati-

ORIGINAL PAGE IS
OF POOR QUALITY

tudes however, where surface albedo stayed fixed, Roads and Vallis found that the lapse rate was stabilized and scaled evaporation fell. Acting alone this would cause cloud cover to fall; however this was compensated for by an increase in the net radiative cooling required to balance the increased precipitation.

Several mechanisms have thus been identified that affect the large-scale cloud and relative humidity fields: (1) eddy vertical velocity, (2) horizontal advection, (3) low-level temperature inversion, (4) radiative effects. How important these mechanisms are for models with more verisimilitude to nature is still unknown. For example, one of the chief simplifications (excepting the GCM work) has been the restriction of clouds to one-level, so prohibiting understanding of the vertical structure of the cloud and relative humidity fields. Since the vertical extent of cloud fields is crucial in determining the relative importance of the solar and infrared radiation components of the radiation field this simplification is ultimately unacceptable. Nor does any wholly satisfactory scheme currently exist, relating cloud cover and cloud optical properties to the dynamical fields (e.g., relative humidity fields) predicted by a GCM.

The study to be described in this paper addresses the problem of the vertical cloud structure using a two-dimensional model with variations in the zonal and vertical directions. The problem of relating clouds to the dynamical and thermodynamical fields is addressed by including an explicit equation for cloud water. The model is written in such a manner that the condensation and radiation algorithms could easily be added to a more comprehensive general circulation model. Some of the suggested hypotheses regarding cloud variability could then be tested further.

2. Model

The model comprises conservation equations for temperature, water vapor, cloud water and parameterizations for the appropriate sources and sinks. The continuous form of the equations may be written:

Thermodynamic

$$\frac{\partial \theta}{\partial t} + \nabla \cdot \underline{v}\theta + \frac{\partial}{\partial p}\omega\theta = g\frac{\partial}{\partial p}F_\theta + \left(\frac{L}{C_p}\dot{C}_\theta\right)p^{-\kappa} + K\nabla^2\theta \qquad (1)$$

Water vapor

$$\frac{\partial q}{\partial t} + \nabla \cdot \underline{v} q + \frac{\partial}{\partial p} \omega q = g \frac{\partial}{\partial p} F_q + \dot{C}_q + K \nabla^2 q \tag{2}$$

Cloud water

$$\frac{\partial c}{\partial t} + \nabla \cdot \underline{v} c + \frac{\partial}{\partial p} \omega c = g \frac{\partial}{\partial p} F_c + \dot{C}_c + K \nabla^2 c \tag{3}$$

Precipitation (steady state form)

$$-F_l = \int_0^p \dot{C}_l \frac{dp}{g} \tag{4}$$

where

θ = potential temperature = $Tp^{-\kappa}$

T = temperature

ORIGINAL PAGE IS
OF POOR QUALITY

$\underline{v}$ = horizontal velocities

ω = pressure velocity

g = gravity

C_p = heat capacity at constant pressure

L = latent heat of condensation and sublimation

q = water vapor mixing ratio

c = cloud water mixing ratio

t = time

$\nabla \cdot$ = horizontal divergence operator

p = pressure

F_θ = thermodynamic eddy + radiative fluxes

F_q = water vapor eddy fluxes

F_c = cloud water eddy fluxes

F_l = precipitation fluxes

$\dot{C}$ = conversion terms for water substance

K = horizontal diffusion coefficient = $10^4 m^2 s^{-1}$

R = perfect gas constant

$\kappa = R/C_p$

ORIGINAL PAGE IS
OF POOR QUALITY

2.1. Numerics

The continuous equations are finite differenced in the horizontal and vertical. The vertical grid consists of points (9) equi-distant in pressure between 1000 and 100 mb. Fictitious boundary points below 1000 and above 100 mb, are used to define values (via boundary conditions) at 1000 and 100 mb. These boundary conditions at 100 mb are

$$\frac{\partial T}{\partial p} = 0$$
$$\frac{\partial q}{\partial p} = 0$$
$$\frac{\partial c}{\partial p} = 0$$
$$\omega = 0$$

and at 1000 mb

$$k\frac{\partial \theta}{\partial p} = k_s(\theta_g - \theta)$$
$$k\frac{\partial q}{\partial p} = \beta k_s(q_g - q)$$
$$k\frac{\partial c}{\partial p} = -k_s c$$
$$\omega = 0$$

where β, k and k_s are empirical coefficients and will be explained later.

Sixteen equally spaced gridpoints are used to represent variations in the zonal direction, and periodic boundary conditions are imposed. In the north-south direction the model currently assumes no variation.

The equations are stepped forward in time using a leapfrog and periodic restart scheme for the dynamical terms and a forward step for the parameterizations. It was found necessary to filter the temperature and moisture in the horizontal to remove 2 gridpoint waves. The condensation routines are then called in order to maintain convective stability and remove any supersaturation.

The velocity fields are preset and remain constant throughout the integration. In addition to a constant zonal wind of constant shear, a divergent wind is also included such that with the pressure velocity the mass continuity equation is satisfied. That is

ORIGINAL PAGE IS
OF POOR QUALITY

$$\nabla \cdot \underline{v} = -\frac{\partial \omega}{\partial p}$$

and $\omega=0$ at the top and bottom is imposed. The imposition of two-dimensionality and fixed velocity fields are the primary simplifications of this model. The paper thus becomes a study of the relationship of cloud structure to a given dynamical field. Complete verisimilitude is sacrificed in the interests of isolating perticular mechanisms. Clearly the dynamical effects and feedbacks of cloud systems on the large-scale must be neglected (e.g., Moncrieff and Green, 1972; Stevens and Lindzen, 1978).

2.2. Vertical eddy fluxes and diabatic heating

The surface fluxes of heat, moisture and cloud-water are described by simple bulk aerodynamic laws

$$F_\theta = k_s(\theta_g - \theta)$$
$$F_q = \beta k_s\ (q_g - q)$$
$$F_c = k_s(-c)$$

where β, which is set to unity here, is related to soil moisture. Further up in the atmosphere the diffusive fluxes are

$$F_\theta = k\frac{\partial \theta}{\partial p}$$
$$F_q = k\frac{\partial q}{\partial p}$$
$$F_c = k\frac{\partial c}{\partial p}$$

The boundary condition used at the surface is that these two fluxes are equal.

The diabatic heating due to radiation is initially parameterized by a Newtonian cooling law

$$g\frac{\partial}{\partial p}F_\theta(rad) = (\theta_e - \theta)/10^6 s$$

More elaborate radiative parameterizations (i.e., Lacis and Hansen (1976) for solar and Rodgers (1967) for infrared) will be incorporated in Section 4.

2.3. Water conversions and convection

The cloud water conversion and precipitation parameterizations are essentially based on simplifications of physically based schemes. A comprehensive treatment of the more complex theory is

ORIGINAL PAGE IS
OF POOR QUALITY

given by Kessler (1969). Here we assume that elaborate microphysical and eddy transport schemes are unnecessary and that the transports of water vapor and temperature are accomplished by large-scale advection or can be adequately parameterized by a convective adjustment scheme.

The conversion terms, $\dot{C}$, are complex nonlinear terms that describe the conversion between water vapor and liquid water or ice and the conversions between different number densities and size distributions. The conversion in this model is simplified by the perhaps rather arbitrary distinction between water/ice droplets of very small diameter and negligible fall velocity (cloud water) and water/ice droplets of large diameter and a substantial fall velocity (precipitation).

2.3.1. Conversion of cloud water to precipitation

The following processes are thought to be the dominant contributors to the conversion of cloud water to precipitation. Initially, small cloud droplets self-collect to form larger cloud droplets and small precipitation particles in a process referred to as auto-conversion by Kessler. The process seems to have a cubic dependence upon cloud water. The so-called Bergeron process also contributes to the formation of small precipitation particles by augmenting ice particles at the expense of liquid water in addition to sublimating water vapor. Presumably this process decreases the auto-conversion time scales. Once small precipitation particles are formed, they fall through the cloud and further collect cloud droplets. This is referred to as accretion and is dependent upon the amount of cloud water and precipitable water as well as their respective number densities and size distributions. In the limit of large accretion, cloud water is probably converted to precipitation as the 4.5 power of cloud water.

It would thus seem that precipitation is converted to cloud water in a highly nonlinear fashion (see also Sundqvist, 1981). This insures that clouds have a fairly uniform mixing ratio (compared to, say, the mixing ratio for water vapor) that precipitation falls from only dense clouds, and that drastic changes in the circulation parameters are only likely to give small changes in the cloud water. For this study we feel it is adequate to use a simple conversion rate, namely

$$\dot{C}_{cl} = ac^3 \tag{5}$$

where $a = 10^4 s^{-1}$. If the precipitation rate is typically $1.9x10^{-5} kgm^{-2}s^{-1}$ then the average cloud water mixing ratio is $5.7x10^{-5} kg/kg$. If clouds exist in only 50% of the atmosphere then the average cloud

water content in the clouds is $7.2x10^{-5}$ and the average cloud water content (cloudy + noncloudy regions) is $3.6x10^{-5}$. These estimates of cloud water content are all within Sasamori's (1975) estimates. The multiplying factor and exponent will be tested later to determine the sensitivity of the model to the cloud physics parameterization. As will be shown, the parameterization is crucial for determining the characteristics of the cloudwater but negligible for determining the cloud fractional cover and large-scale vapor fields. This occurs chiefly at the lower levels because the amount of cloudwater in the atmosphere is negligible compared to the amount of water vapor.

Because of the highly nonlinear rate at which cloud water is converted to precipitation and the desire to maintain a fairly large time-step sufficient only for large-scale dynamical stability, it is assumed that the process can be described as

$$\dot{C}_{cl} = -\int_{t}^{t+\Delta t} ac^3 dt$$

or

$$\dot{C}_{cl} = \frac{c}{\Delta t}\left(1 - \frac{1}{(1+2\Delta t ac^2)^{1/2}}\right) \tag{6}$$

2.3.2. Conversion of precipitation and cloud water to water vapor

Once precipitation is formed it falls through the cloud and into the free atmosphere. If the precipitation is falling in a region of unsaturated air then the precipitation is assumed to evaporate completely or to the point where the air is just saturated. That is, the following set of equations are solved

$$C_p \delta T + L\delta q = 0$$

$$q + \delta q = q^*(T,p) + \frac{\partial q^*}{\partial T}\delta T$$

$$\delta q - \Delta t \frac{g\delta F_l}{\Delta p} = 0$$

where δ denotes the differential changes and an * denotes saturation values (saturation is over water for temperatures above freezing and is over ice for temperatures below freezing). The conversion of precipitation to water vapor is

$$\dot{C}_{lq} = \frac{(q^* - q)}{\Delta t\left(1 + \frac{L\delta q^*}{Cp\delta T}\right)}$$

ORIGINAL PAGE IS
OF POOR QUALITY

ORIGINAL PAGE IS
OF POOR QUALITY

If this results in $-(F_l + \delta F_l) < 0$ then the precipitation is completely evaporated without saturating the atmosphere and the conversion is

$$\dot{C}_{lq} = -\frac{g}{\Delta p} F_l \ .$$

Cloud water in unsaturated conditions is treated in a similar manner to give $\dot{C}_{cq}$.

2.3.3. Conversion of water vapor to cloud water

The conversion of water vapor to cloud water requires simply that supersaturation is reduced to a saturation value instantaneously; hence for supersaturation conditions the following set of equations is solved

$$C_p \delta T + L \delta q = 0$$

$$q + \delta q = q^*(T,p) + \frac{\partial q^*}{\partial T} \delta T$$

or

$$\dot{C}_{qc} = \frac{(q - q^*)}{\Delta t \left(1 + \frac{L}{C_p} \frac{\partial q^*}{\partial T}\right)}$$

2.3.4. Convective condensation

Ostensibly the conversion terms have now been parameterized for the model, but one process remains that will alter the condensation process, namely moist convection. As stated by Manabe *et al* (1965) and Sarachik (1980) our knowledge of this process is insufficient to warrant a too detailed parameterization of moist convection. Further, Lindzen *et al* (1982) found that sensitivity experiments with a moist-adiabatic adjustment yielded similar results to experiments with an alternative cumulus cloud model. Thus, we employ a moist convection adjustment scheme, which operates when the vertical gradient of moist static energy is negative. In the adjustment, it is assumed that turbulent processes occur which equilibrate the moist static energy between the levels, maintain saturated conditions, conserve the total energy, and equilibrate the cloud water. Momentum could also be equilibrated in a similar fashion. The equations for two contiguous levels (1 denotes the upper level and 2 the lower level) are:

ORIGINAL PAGE IS
OF POOR QUALITY

$$C_p\delta T_2 + C_p\delta T_1 + L\delta q_2 + L\delta q_1 = 0$$

$$\Delta h + \frac{C_p}{2}(p_1^\kappa + p_2^\kappa)\{\frac{\delta T_2}{p_2^\kappa} - \frac{\delta T_1}{p_1^\kappa}\} + L(\delta q_2 - \delta q_1) = 0$$

$$q_2 + \delta q_2 = q_2^* + \frac{\partial q_2^*}{\partial T}\delta T_2$$

$$q_1 + \delta q_1 = q_1^* + \frac{\partial q_1^*}{\partial T}\delta T_1$$

$$\delta c_1 + \delta c_2 = -(\delta_{q1} + \delta_{q2})$$

$$c_1 + \delta c_1 = c_2 + \delta c_2$$

where the difference in moist static energy between two levels has been defined as

$$\Delta h = \frac{Cp}{2}(p_1^\kappa + p_2^\kappa)\ (\theta_2 - \theta_1) + L(q_2 - q_1)$$

The convective process occurs whenever $\Delta h > 0$ and $(c_1 + \delta c_1 + c_2 + \delta c_2) \geqslant 0$. The process in the model begins by testing and solving contiguous levels from the bottom of the atmosphere and moving upward. Although more than two levels could be solved simultaneously, idealized tests showed that iteration of the above two-level process produced the same results as multi-level systems; hence, for simplicity, only the two-level system is used. Also, since the time stepping was sufficiently small (approximately 1 hour), iterations at each time step produced the same results as no iterations. However, if the condensation routines are called infrequently, it becomes necessary to iterate. For rapidly changing dynamical conditions it may also be necessary to iterate.

To summarize the above processes, then, the model initially tests for moist static instability. If instability exists the temperature and moisture content of two levels are adjusted to equalize the moist static energy and convert excess water vapor to cloud water. The convection is assumed to equalize cloud water mixing ratio in the vertical. This is repeated through the depth of the atmosphere. Cloud water is then advected, and converted to precipitation according as (6). The precipitation then falls, either to reach the surface or to be evaporated in non-saturated layers. If no convection occurs, we may still have local cloud water vapor to cloud water conversion, and the precipitation process follows in precisely the same fashion.

Having calculated the new stable state, it becomes necessary to define the condensation and the accompanying turbulent transports. These are given by

$$g\frac{\partial F_{T1}}{\partial p} = \frac{\delta T_1}{\Delta t}$$

$$g\frac{\partial F_{T2}}{\partial p} = \frac{\partial T_2}{\Delta t} - \frac{L}{C_p}\dot{C}_{qc}$$

$$g\frac{\partial Fq_1}{\partial p} = \frac{\delta q_1}{\Delta t}$$

$$g\frac{\partial Fq_2}{\partial P} = \frac{\delta q_2}{\Delta t} + \dot{C}_{qc}$$

$$g\frac{\partial Fc_1}{\partial p} = \frac{\delta c_1}{\Delta t}$$

$$g\frac{\partial Fc_2}{\partial p} = \frac{\delta c_2}{\Delta t} - \dot{C}_{qc}$$

ORIGINAL PAGE IS
OF POOR QUALITY

where

$$\dot{C}_{qc} = -\frac{(\delta q_1 + \delta q_2)}{\Delta t}$$

Dry convection also occurs infrequently whenever $\Delta s = \frac{C_p}{2}(p_1^k + p_2^k)\ (\theta_2 - \theta_1) > 0$. As in the moist convective process, q and c are assumed to be well mixed while conserving the dry static energy.

Having found the various functions, the equations (1, 2, 3) for the time rates of changes due to the conversion and convective terms and the precipitation equation (4) become

$$\frac{\partial \theta}{\partial t} = g\frac{\partial}{\partial p}F_\theta + \{\frac{L}{C_p}(\dot{C}_{qc} - \dot{C}_{cq} - \dot{C}_{lq})\}p^{-k}$$

$$\frac{\partial q}{\partial t} = g\frac{\partial F_q}{\partial p} - \dot{C}_{qc} + \dot{C}_{cq} + \dot{C}_{lq}$$

$$\frac{\partial c}{\partial t} = g\frac{\partial F_c}{\partial p} + \dot{C}_{qc} - \dot{C}_{cq} - \dot{C}_{cl}$$

$$-F_l = \int_0^p (\dot{C}_{cl} - \dot{C}_{lq})\,dp/g$$

3. Experiments (Newtonian cooling)

The experiments with a simple Newtonian cooling scheme are designed to illustrate the effects of changing the horizontal advection, vertical velocity and surface temperature, and to study the effects of incorporating an explicit cloud water equation. The velocity fields consist of a mean zonal wind, plus a zonally varying vertical velocity wave. The velocity fields are not meant specifically to reproduce a particular dynamical situation, but to allow the effects of horizontal and vertical motion to be studied in a simple framework.

Figure 1 shows the vertical profiles of the various constants for the control run. The vertical velocity is a maximum ($1.6x10^{-1} kg\ m^{-1}\ s^{-2}$) at 550 mb and decreases to zero at 1000 and 100 mb. The vertical mixing parameter k decreases from $12.6x10^{-1}$ at 1000 mb to $16.5x10^{-3}$ ($kg^2\ m^{-3}\ s^{-3}$) at 100 mb. The zonally averaged wind increases from 10 at 1000 mb to 28 (ms^{-1}) at 100 mb. Since the divergence is assumed to be zero, the zonal wind also includes a component that varies in x. This component is zero at 550 mb and increases linearly to a wave with an amplitude of $4.46 ms^{-1}$ at 1000 and 100 mb. If the pressure velocity varies as a cosine wave, then u varies as a sine wave with positive amplitude below 550 mb and negative amplitude above.

Because of the constant value of the winds, steady state solutions for the equations are obtained. We will describe in detail the results for the control experiment and then results from other experiments motivated in part by the simple one-level cloud system of Roads (1978b).

Figure 2 shows a steady-state solution as a function of longitude for the control parameters. Here the periodic domain extends from west to east with a distance of $5x10^3$ km and grid points every 312.5 km. Essentially wave #6 phenomenon is studied if these scales are appropriate for midlatitude circulation systems. The vertical velocity wave is shown in the upper part of the figure to have maximum descending motion on the edges of the domain and maximum ascending motion in the center of the domain. The precipitation at the surface is correlated with the vertical motion field although precipitation is certainly narrower, occuring significantly over less than 1/3 of the domain. Note also that the precipitation occurs almost strictly on the leeward side of the vertical velocity wave. The characteristic features suggest that for the chosen parameters, horizontal advection of moist air is extremely important for the precipitation field.

Various measures of the total cloud cover are also shown in Figure 2. Of course, the most natural criterion to use is simply the presence of cloud water, although clearly this cannot be used in GCMs which do not predict cloud water. The narrowest measure is the area of positive condensation which also corresponds with the area of precipitation at the surface. If the presence of cloud water or a relative humidity criterion (H=1) is used then the cloud boundary extends a further distance on the windward side. Smaller relative humidity criterions naturally give larger coverages still.

ORIGINAL PAGE IS
OF POOR QUALITY

ORIGINAL PAGE IS
OF POOR QUALITY

The two-dimensional structure of the cloud, relative humidity and temperature fields are shown in Figure 3a,b,c. First note that the cloud has an eastward tilt with altitude indicating that dry air advection occurs on the windward side and cloud water advection occurs on the leeward side. The relative humidity field gives a good indication of this structure and also shows that a minimum in relative humidity exists below the tropopause. The temperature field is that which would be expected for a forced circulation with the strongest positive deviations eastward of regions of descent and the strongest negative deviations in regions eastward of the ascending regions. The deviations are substantial with a maximum eastward temperature difference of about 15°C indicating differences in heating of $1.5x10^{-5}Ks^{-1}$. Of interest also is that the deviations are negative in the region of the cloud top indicating that the parameterized heating rate is positive in this region.

Various experiments were run to see the contributions and sensitivity of various mechanisms. Figure 4 shows the response when the mean zonal wind is removed. In this case the cloud cover decreases at the lowest level and substantially increases at the upper level. The relative humidity becomes less in the descending regions and the atmosphere becomes relatively warmer in the descending regions. Not much temperature change occurs in regions of ascent except at the top of the cloud where strong negative temperature deviations occur indicating strong radiative heating. Due to this drastic change in circulation pattern, the change in the zonally averaged relative humidity does not correspond to the change in cloud coverage. For example, in the middle levels fractional cloud cover increased while the zonally averaged relative humidity decreased.

Another experiment in which the vertical velocity amplitude was decreased an order of magnitude yielded cloud coverage at all longitudes and levels except for the uppermost level and part of the next uppermost level. Although the decrease in vertical velocity yielded cloud coverage and evaporation everywhere, the precipitation is much less for this case as may be seen in Figure 5. Note also that the precipitation is strongest in the center of the rising motion and much weaker in regions of descent, decreasing to zero in regions of strong descent. Thus the cloud and precipitation characteristics are strongly dependent upon the ability of the atmosphere to dry itself out in addition to being able to produce clouds.

ORIGINAL PAGE IS
OF POOR QUALITY

Another mechanism that is important for latitudinal differences in cloudiness is the mean zonal vertical velocity. Although its inclusion is inconsistent because meridional divergence is not allowed, a term of the form $\overline{\omega}\frac{\partial A}{\partial p}$ was added to the flux $\nabla\cdot\underline{v}A + \frac{\partial}{\partial p}\omega A$, where A is temperature or mixing ratio. $\overline{\omega}$ had the same vertical profile as the eddy vertical velocity term (see Fig. 1) but a much smaller amplitude maximum of $2.5x10^{-2}\ kgm^{-1}s^{-3}$. Because the continuity equation is no longer satisfied, precipitation was much less than evaporation. However, a steady state was reached and is shown in Fig. 6. Note that a low-level cloud of small areal coverage is formed in a very dry and hot atmosphere.

When the surface temperature is varied, large changes in the cloud structure result. Fig. 7a,b show the response in the cloud and relative humidity fields for an increase of surface temperature of 10K and Fig. 7c,d show the response in the cloud and relative humidity fields when the surface temperature is decreased by 10K. Note that clouds strongly increase for a more unstable boundary layer almost everywhere. Also of interest was that the clouds were almost completely formed by moist convection for the unstable boundary case and completely by local supersaturation condensation for the stable boundary case. As discussed by Roads and Vallis (1982) these cases have applications to models in which the ice line is allowed to change, because of large changes in low-level static stability and cloudiness in regions of the ice line.

It was pointed out above that a major difference between this model and others is the explicit inclusion of cloud water. If all cloud water is precipitated out as soon as it forms, then essentially the model reduces to the conventional types. A comparison of cases with and without cloud water and its concomitant advection is useful. Thus three of the above described experiments were rerun with immediate precipitation of cloudwater. For these cases it is shown in Figure 8 that the relative humidity fields are more or less the same with or without cloud water except at the top of the atmosphere where cirrus cloudiness is dependent upon cloud water being present. Because of the large influences that cirrus cloudiness has on the radiation field it would seem to be better to retain the cloudwater parameterizations. However, good estimates of cloud cover in the lower regions are obtained by equating cloud cover to values of relative humdity fields near unity. At the other extreme Figure 9 shows the response when $\dot{C}_{cl} = 10^2c^3$ (as opposed to 10^4c^3 see eq. 5). The cloud water content increases by a

ORIGINAL PAGE IS
OF POOR QUALITY

factor of 5 with the largest areal change occurring at the upper levels where cloud water can now extend over much more extensive regions because of the importance of advection. The change in the relative humidity and temperature field are negligible however at the lower levels. Thus, from the two previous experiments, we conclude that cloud characteristics and variations are determined by the circulation parameters that result in saturation and that modifications to these occur chiefly at upper levels where cirrus clouds detrain from the main cloud. The precise form of the cloud microphysical constants appears unimportant.

The change in the Newtonian heating profile produced some interesting effects. Figure 10 shows the response when the equilibrium temperature was either decreased by 10° everywhere, including the surface, or increased by 10°, including the surface, everywhere. Note that the cloud fields remain about the same in the lower to upper troposphere but that the run with the increased temperature resulted in decreased upper-level cloudiness.

Somewhat different responses occur when the cloud water is totally removed at each time step, Fig. 10a and 10b, because then the amount of upper level cloudiness ($H \geqslant 1$) is actually decreased at the upper levels (except for the topmost level) with decreasing temperature. So if cloudwater is included, the upper levels tend to detrain cloudwater over a longer distance. Presumably this occurs because at the higher temperatures the relative humidity deficit is sufficient to evaporate the cloud water but at lower temperatures the cloudwater (which is maintained at a fairly uniform level by the nonlinear precipitation processes) is much larger than the relative humidity deficit and can travel over much larger distances before finally being evaporated in the driest regions. Thus, if cloudwater is retained in the model, upper level cloudiness will increase with decreasing temperature whereas if cloud water is not retained, upper level cloudiness will increase with increasing temperature.

4. Cloud Radiation Feedbacks

Schemes for calculating the infrared and solar radiation fluxes were incorporated in order to allow a more self-consistent model. The schemes are fully interactive in that the water vapor and cloud water content predicted by the model are used in the radiative calculations.

ORIGINAL PAGE IS
OF POOR QUALITY

4.1. Infrared radiation

The infrared scheme is based on the emissivity approximation (see Rodgers, 1967), in which the integration over all spectral wavelengths is incorporated into simple transmission formulas. In terms of transmissivity the equations are

$$F\uparrow(p) = \int_{\tau(p_s,p)}^{1} B(p')d\tau(p,p') + B_g\tau(p_s,p)$$

$$F\downarrow(p) = -\int_{1}^{\tau(p,0)} B(p')d\tau(p,p')$$

where

$F\uparrow(p)$ = the upward flux

$F\downarrow(p)$ = the downward flux

$\tau(p,p')$ = transmissivity between p and p'

$B(p)$ = $\sigma T^4(p)$

$T(p)$ = absolute temperature

σ = Stefan-Boltzmann constant

B_g = σT_g^4

T_g = surface temperature

The transmissivity for water vapor is taken from Rodgers. Carbon dioxide is accounted for by assuming that the total transmissivity is the product of the transmissivity of H_20 and CO_2 where

$$\tau(CO_2) = .926 - .02\ ln(\Delta u)$$
$$\Delta u = 120\frac{\Delta p^2}{p_s^2}$$

where p_s is the surface pressure and Δp^2 is the pressure squared differential (using a value of 120 implies a CO_2 content of approximately 300 ppm). Thus Δu is a pressure weighted path length. In a

ORIGINAL PAGE IS
OF POOR QUALITY

similar manner, the transmissivity in the presence of cloud is the product of cloud, H_2O and CO_2 transmissivities. Currently the cloud transmissivity is taken to be

$$\tau = 1 - u/a; u < a$$
$$\tau = 0; u \geq a$$

where

$$du = c\frac{dp}{g}$$
$$a = 3x10^{-2} kg\ m^{-2}$$

The dependence of τ on u produces nearly black clouds everywhere except at the cirrus levels. For example, at the uppermost level the typical c is on the order of $1x10^{-5} kg/kg$ and the typical τ is on the order 2/3.

4.2. Solar radiation.

The solar radiation scheme uses the multiple scattering method described by Lacis and Hansen (1974) and Somerville *et al* (1974). Simplified two stream approximations and absorption coefficient approximated by a sum of 6 gray absorbing intervals are used in partially cloudy skies. In an entirely clear sky and above the highest clouds the absorption is calculated using an integrated absorption coefficient. In this study single layer optical depths are assumed to be given by

$$\tau = c\frac{\Delta p}{g} 10^2$$

The typical optical depth in the lower layers is then around 8 for a pressure interval of 100 mb and a cloudwater mixing ratio of $8x10^{-5}$ kg/kg. In the upper-most layers the optical depth is about 1 for a pressure interval of 100 mb and a cloudwater mixing ratio of $1x10^{-5}$ kg/kg.

As a typical cosine zenith angle we use $\mu = .225$ which is appropriate for the annually and diurnally averaged zenith angle at 45° latitude. The solar constant is set at 1372 W/m^2.

4.3. Surface temperature

The surface temperature equation can be written in the form

$$C_g \frac{\partial T_g}{\partial t} = F_T\downarrow + S\downarrow - \sigma T_g^4 - LE - S_H$$

ORIGINAL PAGE IS
OF POOR QUALITY

where

$F_T\downarrow$ = downcoming infrared radiation

$S\downarrow$ = net downward solar flux

E = evaporation flux

S_H = sensible heat flux

C_g = surface heat capacity

At present a very small surface heat capacity is used ($C_g = 3x10^3\ Jm^{-2}$) so that the temperature is determined mainly as a flux balance between the outgoing evaporation, sensible heat, and infrared flux and incoming solar and infrared radiation fluxes. The equation is time differenced implicitly so that no instability develops.

4.4. Experiments

The equilibrium profiles of cloud water, relative humidity and temperature are given in Figure 11. The major differences between the previous cases is that the lower boundary tends to be more unstable which produces cloud at the lower levels everywhere the motion is upward. The upper level cloud field is similar however.

The radiation cooling rates, $\frac{\partial\theta}{\partial t}$, are shown next in Figure 12. Immediately noticeable is that in the atmosphere infrared radiation is dominant especially near the cloud boundaries. Above the lower level clouds, cooling rates of up to 15°/day can occur whereas below the upper level clouds heating rates up to 6°/day can occur. In contrast is the surface flux balance shown in Figure 13. Here it is the solar flux that varies most strongly from east to west with substantially less radiation below the clouds. This solar radiation variation is balanced by an increase in downward radiation, a decrease in upward radiation and decreased sensible and latent heat fluxes to the atmosphere.

Figure 14 shows the response when the cloud radiation feedbacks are modified. Here the model was only integrated for 30 days and although the solution had not yet reached a steady state the solution was in a statistically stationary state and was converging slowly toward equilibrium with a slowly increasing exponential damping rate of >30 days. Note that in the absence of cloud radiation feed-

ORIGINAL PAGE IS
OF POOR QUALITY

backs the temperature increases almost everywhere except at the upper levels. In the presence of infrared radiation feedbacks alone the atmosphere is still warmer, demonstrating the cloud greenhouse effect. Solar radiation, however, dominates the total cloud radiation feedback and this model atmosphere tends to be colder because of clouds. These results are similar to results found with the GLAS GCM (Herman *et al*, 1980).

Finally, we show a calculation for the response of the model atmosphere to a quadrupling of CO_2. This amount of CO_2 increase is well within current projections (Bolin *et al*, 1981) which show that by the end of the 23rd century the atmosphere could contain 4 to 8 times present amounts. Two experiments were run to test the effect of the clouds on the solution. In the fixed cloud, FC, experiment, the clouds which interacted with the radiation field were the clouds found from the control run. In the variable cloud experiment the clouds were allowed to change and interact with the radiation field. The time variation of the two runs for an arbitrary surface temperature is shown in Figure 15. Note that the variable cloud experiment produces a shorter convergence time than the one with fixed clouds, indicating a negative feedback.

The change in the cloud field is shown in Figure 16. Note that the upper level cloudiness tends to decrease, and cloud cover at the eastern and western side of the original system also tends to fall in spite of the general overall increase in cloud water in the center of the cloud. In fact, the one positive region on the left edge of the cloud was substantial, increasing by $7x10^{-5}$ and strongly increasing the infrared cooling in this region. As shown in Figure 17, this change in cloudwater decreases the albedo of the atmosphere indicating that the quadrupling of CO_2 causes slightly more absorption of solar radiation for the variable cloud experiment than the fixed cloud experiment. However, because of the increased water vapor content the albedos are reduced in both cases.

Figure 18 shows the zonally averaged potential temperature response for a CO_2 quadrupling for the fixed and variable cloud experiments. In the variable cloud experiments the quadrupling produced a potential temperature change of about 2°K at the surface increasing to about 4K at 50kPa and then decreasing in the upper troposphere with an overall increase in potential temperature. In the lower to mid troposphere the fixed cloud experiments showed similar albeit larger responses and in the upper

ORIGINAL PAGE IS
OF POOR QUALITY

troposphere the responses are completely opposite with the fixed cloud experiments showing a very strong increase in potential temperature.

In the fixed cloud experiments the vertical temperature structure tended to change according to changes in the moist adiabatic lapse rate. However, in the variable cloud experiments temperature responded similarly up to about 40kPa but then the temperature change decreased rapidly. Presumably, the decrease in upper level cloudiness has a strong influence on the results of the variable cloud experiments: reduction in upper level cloudiness allows radiation from lower in the atmosphere to more easily escape to space.

This experiment shows that assumptions about cloudiness can have a large influence upon the sensitivity of the upper troposphere, and to a smaller degree the lower tropospheric response. In this respect we are reminded of the experiments of Weare and Snell (1974) which also showed a reduced sensitivity to CO_2 because of their cloud model assumptions. (See also Charlock, 1982; Paltridge, 1980.)

5. Conclusions

This study has been concerned with the relationship of cloud fields with various features of atmospheric circulation patterns. In particular we have examined the effects of explicitly including cloud water and the effects on cloud cover of increasing temperature with increased atmospheric carbon dioxide. We have also considered the effects of variations in horizontal and vertical advection.

The effect of including cloud water is clearly seen only at the uppermost levels. At mid and lower levels, cloud cover is very well correlated with the relative humidity and condensation fields. Only at upper levels, where advection of cloud water over large distances can occur, does its explicit inclusion make a qualitative difference. Further, the cloud cover is not strongly dependent on the particular microphysical parameterizations used, although the cloud water content (and hence the albedo) of the atmosphere is. When the temperature is altered, cloud cover generally responds in a similar fashion as relative humidity, except at upper levels. With cloudwater, the upper-level cloud cover tends to decrease with increased temperature because enhanced evaporation of cloud water prevents extensive

ORIGINAL PAGE IS
OF POOR QUALITY

advection. However, with no cloudwater, relative humidity increased with increasing temperature at the upper levels.

The incorporation of a fully self-consistent radiative model did not essentially alter these conclusions. The cloud field that developed was similar to the ones which used Newtonian cooling although it was slightly larger at the lower levels. It was shown that infrared radiation was most important for determining the atmospheric temperature structure whereas solar radiation was most important for determining surface variations. If the cloud radiation feedbacks were excluded then the model atmosphere warmed slightly albeit much less than if only the solar radiative feedbacks were excluded. This indicates that the infrared and solar cloud feedbacks were almost compensatory but that the solar radiation feedback was slightly stronger.

On the other hand, in a sensitivity experiment in which the CO_2 was quadrupled the dominant feedback was the infrared component. Increasing CO_2 levels warmed the atmosphere and generally decreased upper level cloud cover, but increased cloud water content slightly at mid levels. Mid level areal cloud cover was little changed. The reduction in upper level cloud cover caused a reduction in the cloud-greenhouse effect (larger than any albedo effect) and reduced the total warming, compared with the case in which cloud cover was fixed. It would thus seem that the explicit incorporation of cloud water is necessary to predict correctly the response to CO_2 changes. In this model, clouds act to reduce the sensitivity of the model response to CO_2 perturbations.

The relationship of the cloud cover to the dynamical fields are generally consistent with the previous pictures obtained using one-level systems (e.g., Roads, 1978b). Thus, areal cloud cover is increased by decreasing eddy vertical velocity, increasing the mean upward vertical velocity, decreasing the zonal advection.

Finally we mention again some of the limitations of this model. The main simplifications lie in the assumption of two-dimensionality and in not allowing the large-scale cloud systems to change the winds in response to temperature changes. Thus the increased temperature - increased intensity of hydrology cycle - increased vertical velocity - reduced cloud cover feedback was not included in the CO_2 experiments. Further, the stratosphere was assumed to be an isothermal layer over an active

troposphere. The relaxation of such assumptions within the framework of a simple model will be an important next step in understanding the cloud and climate response to changes in external forcing.

ORIGINAL PAGE IS
OF POOR QUALITY

Acknowledgments

This research was funded in part by Calspace. J. O. Roads was also supported by NASA grant NAG5-105. Helpful comments were given by R. Somerville and C. Gautier of Scripps and G. Diak of Wisconsin. The manuscript was expertly text-edited by G. Johnston and the figures expertly drafted by F. Crowe.

ORIGINAL PAGE IS
OF POOR QUALITY

ORIGINAL PAGE IS
OF POOR QUALITY

References

Bolin, G., A. Björkstrom, C. D. Keeling, R. Bacastow, U. Siegenthaler, 1981: In *Carbon Cycle Modelling*, Edited by Bolin, John Wiley & Sons, 1-28.

Cess, R. D., 1976: Climate change: An appraisal of atmospheric feedback mechanisms employing zonal climatology. *J. Atmos. Sci., 33*, 1831-1843.

Cess, R. D. and V. Ramanathan, 1978: Averaging of infrared cloud opacities for climate modeling. *J. Atmos. Sci., 35*, 919-922.

Cess, R. D., B. P. Bruglel and M. S. Liam, 1982: Low latitude cloudiness and climate feedback. Comparative estimates from satellite data. *J. Atmos. Sci., 39*, 53-59.

Charlock, T. P., 1982: Cloud optical feedback and climate stability in a radiative convective model. *Tellus, 34*, 245-254.

Hartmann, D. L. and D. A. Short, 1980: On the use of earth radiation budget statistics for studies of clouds and climate. *J. Atmos. Sci., 37*, 1233-1250.

Herman, G. F. , M. C. Wu and W. Johnson, 1980: The effect of clouds on the earth's solar and infrared radiation budgets. *J. Atmos. Sci., 37*, 1251-1261.

Kessler, F., 1969: On the distribution and continuity of water substance in atmospheric circulations. *Meteorological Monographs, 10*, Amer. Met. Soc., 84 pp.

Lacis, A. A. and J. E. Hansen, 1974: A parameterization for the absorption of solar radiation in the earth's atmosphere. *J. Atmos. Sci., 31*, 118-133.

Lindzen, R. S., A. Y. Hou and B. F. Farrell, 1982: The role of convective model choice in calculating the climate impact of doubling CO_2. *J. Atmos. Sci., 39*, 1189-1205.

Ludlum, F. H., 1980: *Clouds and Storms*, Pennsylvania State Univ. Press, 405 pp.

Manabe, S. and R. T. Wetherald, 1975: The effects of doubling the CO_2 concentration on the climate of a general circulation model. *J. Atmos. Sci., 32*, 3-15.

Manabe, S., J. Smagorinsky and R. F. Strickler, 1965: Simulated climatology of a general circulation model with a hydrologic cycle. *Mon. Wea. Rev., 93*, 769-798.

Moncrieff, M. W. and J. S. A. Green, 1972: The propagation and transfer properties of steady

ORIGINAL PAGE IS
OF POOR QUALITY

convective overturning in shear. *Q. J. Roy. Met. Soc., 98*, 336-357.

Ohring, G., and P. Clapp, 1980: The effect of changes in the cloud amount on the net radiation at the top of the atmosphere. *J. Atmos. Sci., 37*, 447-454.

Paltridge, G. W., 1980: Cloud radiation feedback to climate. *Q. J. Roy. Met. Soc., 106*, 895-899.

Potter, G. L., H. W. Ellsaesser, M. C. MacCracken and C. S. Mitchell, 1981: Climate change and cloud feedback: The possible radiative effects of latitudinal redistribution. *J. Atmos. Sci., 38*, 489-493.

Roads, J. O., 1978a: Numerical experiments on the climatic sensitivity of an atmospheric hydrologic cycle. *J. Atmos. Sci., 35*, 753-773.

Roads, J. O., 1978b: Relationships among fractional cloud coverage, relative humidity and condensation in a simple wave model. *J. Atmos. Sci., 35*, 1450-1462.

Roads, J. O. and G. K. Vallis, 1982: An energy balance climate model with cloud feedbacks. (submitted)

Rodgers, C. D., 1967: The use of emissivity in atmospheric radiation calculations. *Q. J. Roy. Met. Soc., 93*, 43-54.

Sarachik, E., 1980: Cloud generation in climate models. In Clouds in Climate: Modeling and Satellite observational Studies. Report of Workshop held at NASA Goddard Institute for Space Studies, New York, NY, Oct 29-31, 1980.

Sasamori, T., 1975: A statistical model for stationary atmospheric cloudiness, liquid water content and rate of precipitation. *Mon. Wea. Rev., 103*, 1037-1049.

Schneider, S. H., 1972: Cloudiness as a global climate feedback mechanism. The effects on the radiation balance and surface temperature of variations in cloudiness. *J. Atmos. Sci., 29*, 1413-1422.

Schneider, S. H., W. M. Washington and R. M. Chervin, 1978: Cloudiness as a climate feedback mechanism: Effects on cloud amounts of prescribed global and regional surface temperature changes in the NCAR GCM. *J. Atmos. Sci., 35*, 2207-2221.

Shukla, J. and Y. Sud, 1981: Effect of cloud-radiation feedback on the climate of a general circu-

lation model. *J. Atmos. Sci., 38*, 2337-2353.

Smagorinsky, J., 1960: On the dynamical prediction of large scale condensation by numerical methods. *Geophys. Monogr., 5*, Am. Geophys. Union, 71-78.

Somerville, R. C. J., P. H. Stone, M. Halem, J. E. Hansen, J. S. Hogan, L. M. Druyan, G. Russel, A. A. Lacis, W. J. Quirk and J. Tenenbaum, 1974: The GISS model of the global atmosphere. *J. Atmos. Sci., 31*, 84-117.

Sundqvist, H., 1981: Prediction of stratiform clouds: Results from a 5-day forecast with a global model. *Tellus, 33*, 242-253.

Stevens, D. E. and R. S. Lindzen, 1978: Tropical wave - CISK with a moisture budget and cumulus friction. *J. Atmos. Sci., 35*, 940-961.

Vallis, G. K., 1982: A statistical-dynamical climate model incorporating a simple hydrology cycle. *Tellus, 34*, 211-227.

Wetherald, R. T. and S. Manabe, 1980: Cloud cover and climate sensitivity. *J. Atmos. Sci., 37*, 1485-1510.

ORIGINAL PAGE IS
OF POOR QUALITY

ORIGINAL PAGE IS
OF POOR QUALITY

Figure Legends

Figure 1 Vertical structure of various control parameters. A denotes a general component for either $\overline{\omega}$, $u-10$, k, ω and the multiplying factor is denoted on the figure. The temperature scale for T_e, θ_e is given at the top of the figure. All values are in mks units.

Figure 2 Zonal structure of various components as a function of I, the zonal gridpoint running from east to west. ω denotes the eddy pressure velocity, $\dot{P}$ the precipitation rate, and E the evaporation rate in $kg\ m^{-2}\ s^{-1}$. Various measures of the total cloud cover; C, cloudwater > 0; C+, condensation > 0; $H \geqslant 1$; $H \geqslant .9$ are also given.

Figure 3a The two-dimensional structure of the cloudwater for the control case. Contours are every 0, 4, $8x10^{-5}$ kg/kg.

b Same as 3a except for relative humidity. Contours cover the range 30% to 90%.

c Same as 3a except for deviations of potential temperature field from the radiative equilibrium values. Contours are every 5 degrees and positive values indicate Newtonian cooling and negative values indicate Newtonian heating.

Figure 4 Same as 3 except $\overline{u} = 0$.

Figure 5 Zonal structure of the precipitation and evaporation for the cases $\overline{u} = 0$ and $\omega = .1\omega$ (control).

Figure 6 Same as 3 except $\overline{\omega} = 2.5x10^{-2}$.

Figure 7a Same as 3a except $T_g = T_g$ (control) + 10.

b Same as 3b except $T_g = T_g$ (control) + 10.

ORIGINAL PAGE IS
OF POOR QUALITY

c Same as 3a except $T_g = T_g$ (control) - 10.

d Same as 3b except $T_g = T_g$ (control) - 10.

Figure 8a Same as 3b except cloudwater is totally precipitated.

b Same as 4b except cloudwater is totally precipitated.

c Relative humidity field for case where $\omega/10$ is used and cloudwater totally precipitated.

Figure 9 Same as 3 except $\dot{C}_{cl} = c^3 x 10^2$.

Figure 10a Same as 3a except $\theta_e = \theta_e$ (control) + 10 and $T_g = T_g$ (control) + 10.

b Same as 3b except $\theta_e = \theta_e$ (control) + 10.

c Same as 10b except for experiment in which all cloudwater is precipitated.

d Same as 3a except $\theta_e = \theta_e$ (control) - 10 and $T_g = T_g$ (control) - 10.

e Same as 3b except $\theta_e = \theta_e$ (control) - 10 and $T_g = T_g$ (control) - 10.

f Same as 10e except for experiment in which all cloud water is precipitated.

Figure 11 Control run for model with cloud radiative feedbacks.

a cloudwater with contours at 0, 1, 2, 4, 8 x 10^{-5} kg/kg.

b relative humidity field.

c potential temperature field minus the zonal mean temperature.

Figure 12 Control run for model with cloud radiative feedbacks.

a infrared heating rates, $\frac{\partial \theta}{\partial t}$, with contours every 4, 2, 1, 0,-1,-2,-4,-8 x 10^{-5} K^{-1}

b solar heating rates, $\frac{\partial \theta}{\partial t}$, with contours every .25, .5, .75, 1 x 10^{-5} $K\ s^{-1}$.

Figure 13 Surface fluxes in watts m^{-2}. Positive values increase surface temperature and negative values decrease surface temperature. $F_T\downarrow$, S, SH,E, $F_T\uparrow$ refer to downward thermal radiation, downward solar radiation, sensible heat,

evaporation, and upward thermal radiation. Also shown are the surface temperature T_g and planetary albedo α.

Figure 14 Change in temperature after 30 days for the experiment with no cloud radiation feedbacks, $\Delta\theta_N$, and no solar-cloud radiation feedbacks, $\Delta\theta_{NS}$. The latter experiment includes infrared feedbacks.

Figure 15 Fixed cloud, FC, and variable cloud, VC, temperature changes due to CO_2 quadrupling, as a function of time. Both experiments were initialized from the end of the control run.

Figure 16 Differences in cloud field for VC CO_2 experiment minus control. Only plus and minus values are indicated because of the large variance of cloud water concentrations. In the negative region at the top of the cloud the maximum cloud water change is $-1.1x10^{-5}$ kg/kg.

Figure 17 Change in planetary albedo for sensitivity experiments minus the control run. With the exception of one small area for the valuable cloud experiment, the albedo change is negative indicating that model atmosphere absorbs more solar radiation with increased CO_2.

Figure 18 Vertical structure of the potential temperature change (perturbed minus control) induced by CO_2 quadrupling for the fixed cloud experiments at 60, 120, 180, 360 days (FC60, FC120, FC180, FC360) and the variable cloud experiments at 60, 120, 180 days (VC60, VC120, VC180)..

ORIGINAL PAGE IS
OF POOR QUALITY

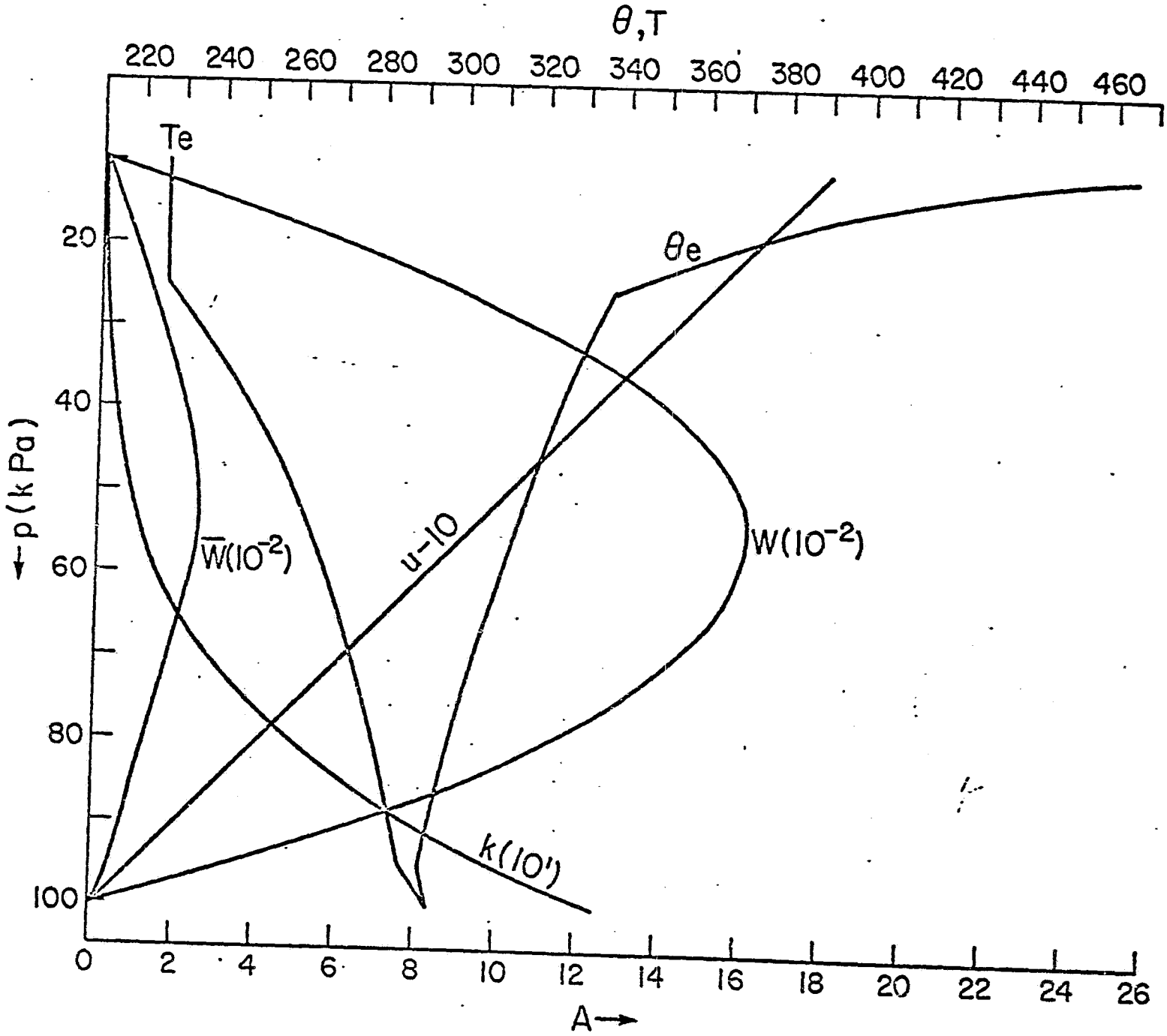

Figure 1

ORIGINAL PAGE IS
OF POOR QUALITY

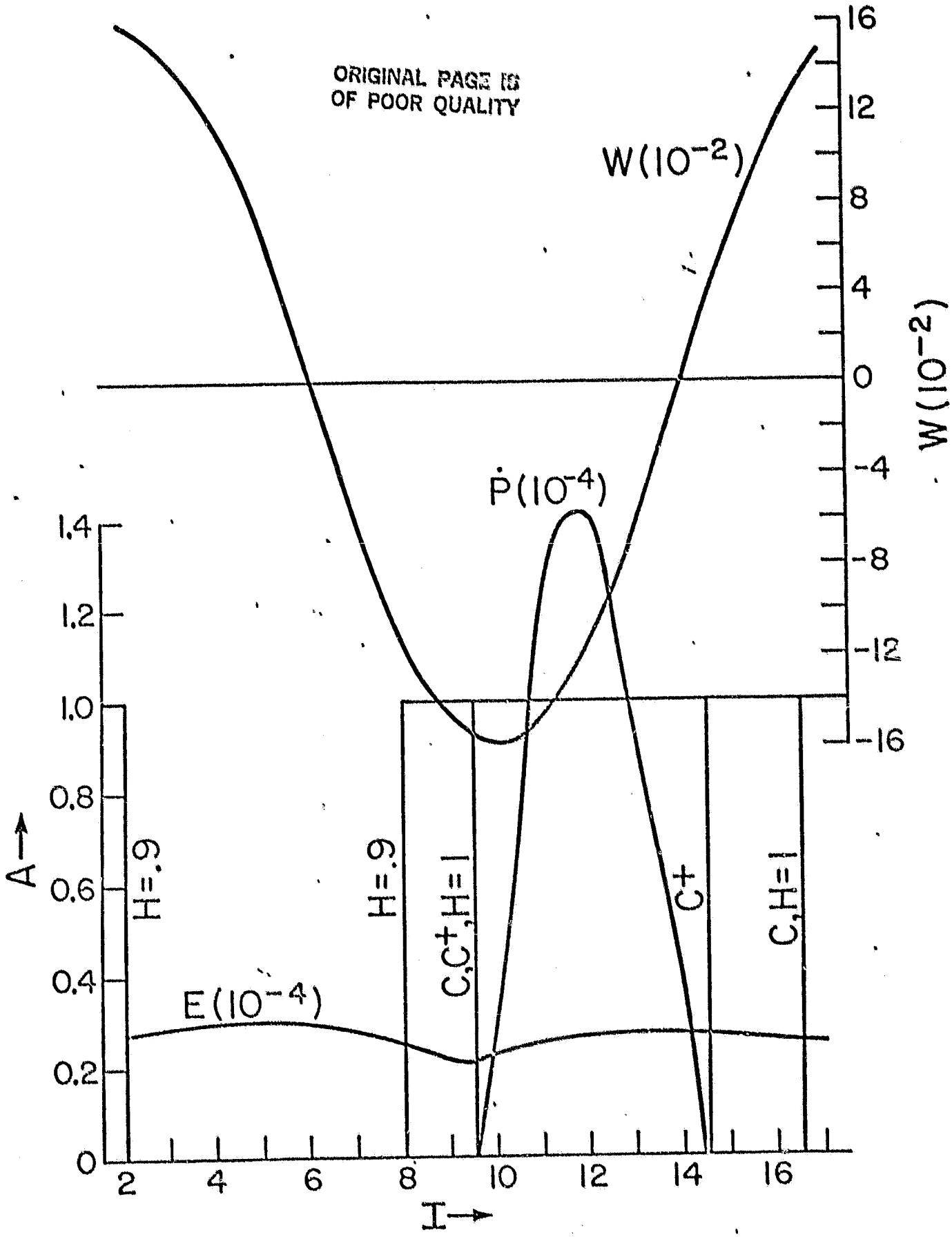
ORIGINAL PAGE IS
OF POOR QUALITY
W(10^-2)
Ṗ(10^-4)
E(10^-4)
H=.9
H=.9
C,C+,H=1
C+
C,H=1
A→
I→
W(10^-2)
16
12
8
4
0
-4
-8
-12
-16
1.4
1.2
1.0
0.8
0.6
0.4
0.2
0
2
4
6
8
10
12
14
16

Figure 2

ORIGINAL PAGE IS
OF POOR QUALITY

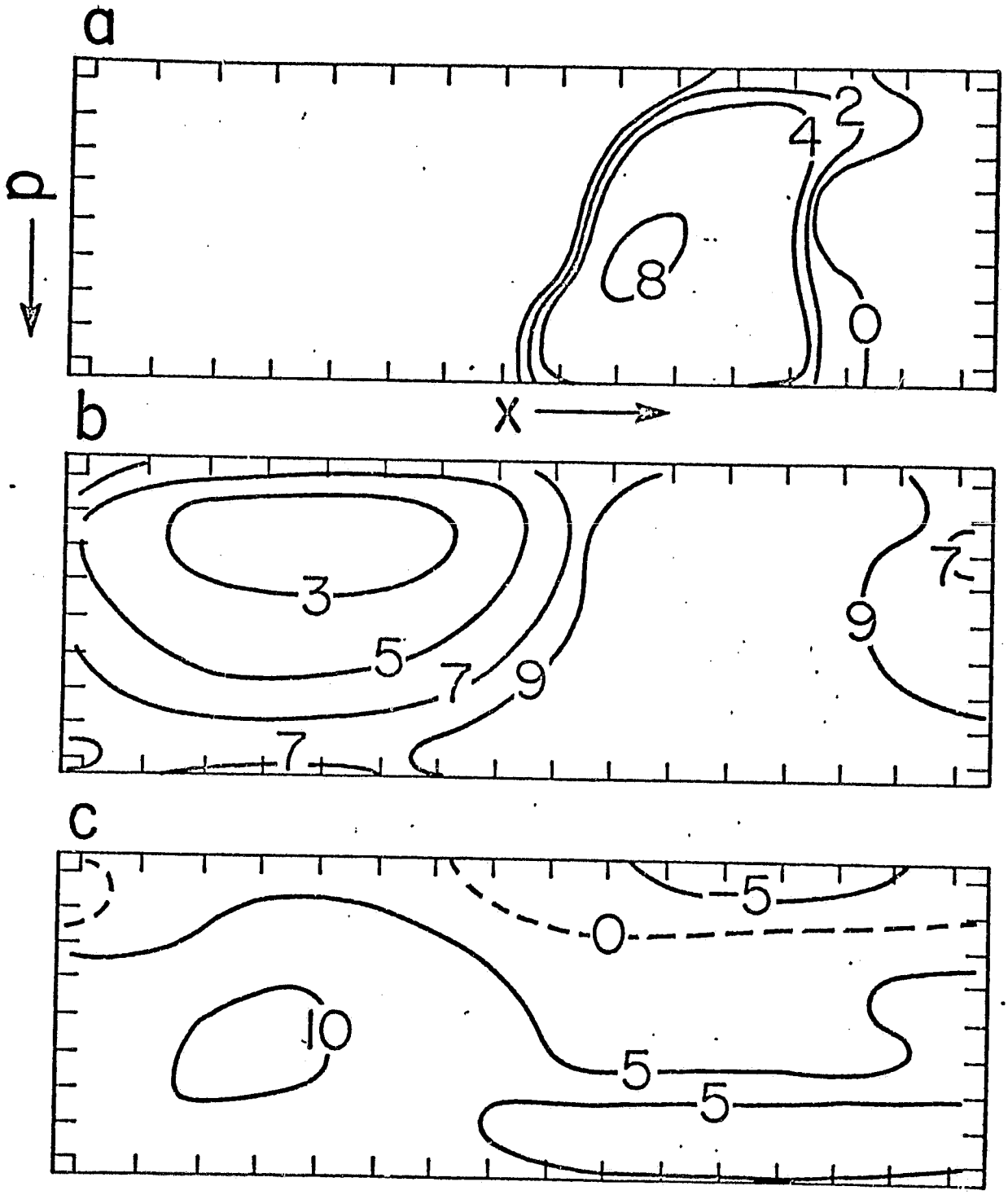

Figure 3

ORIGINAL PAGE IS
OF POOR QUALITY

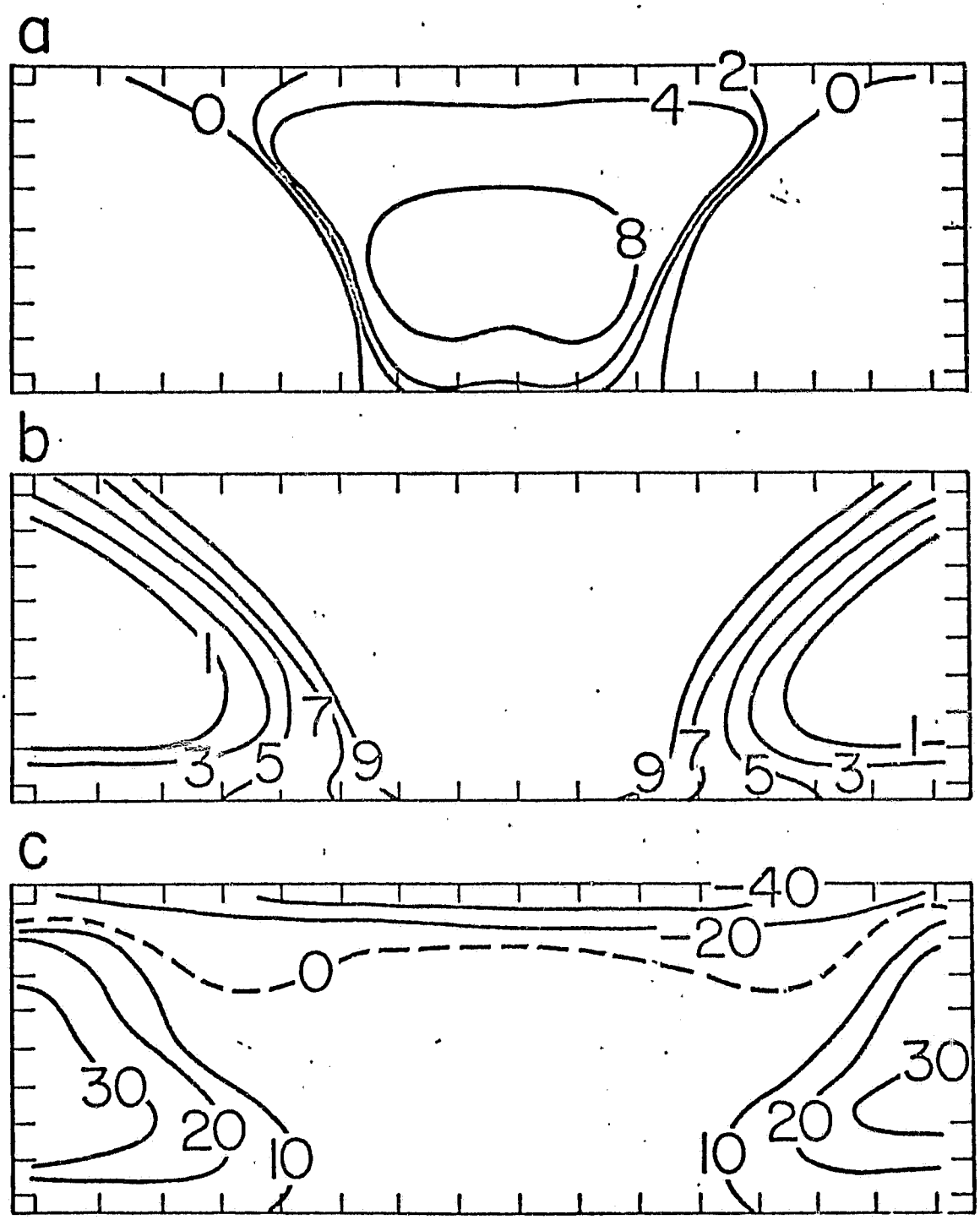

Figure 4

ORIGINAL PAGE IS
OF POOR QUALITY

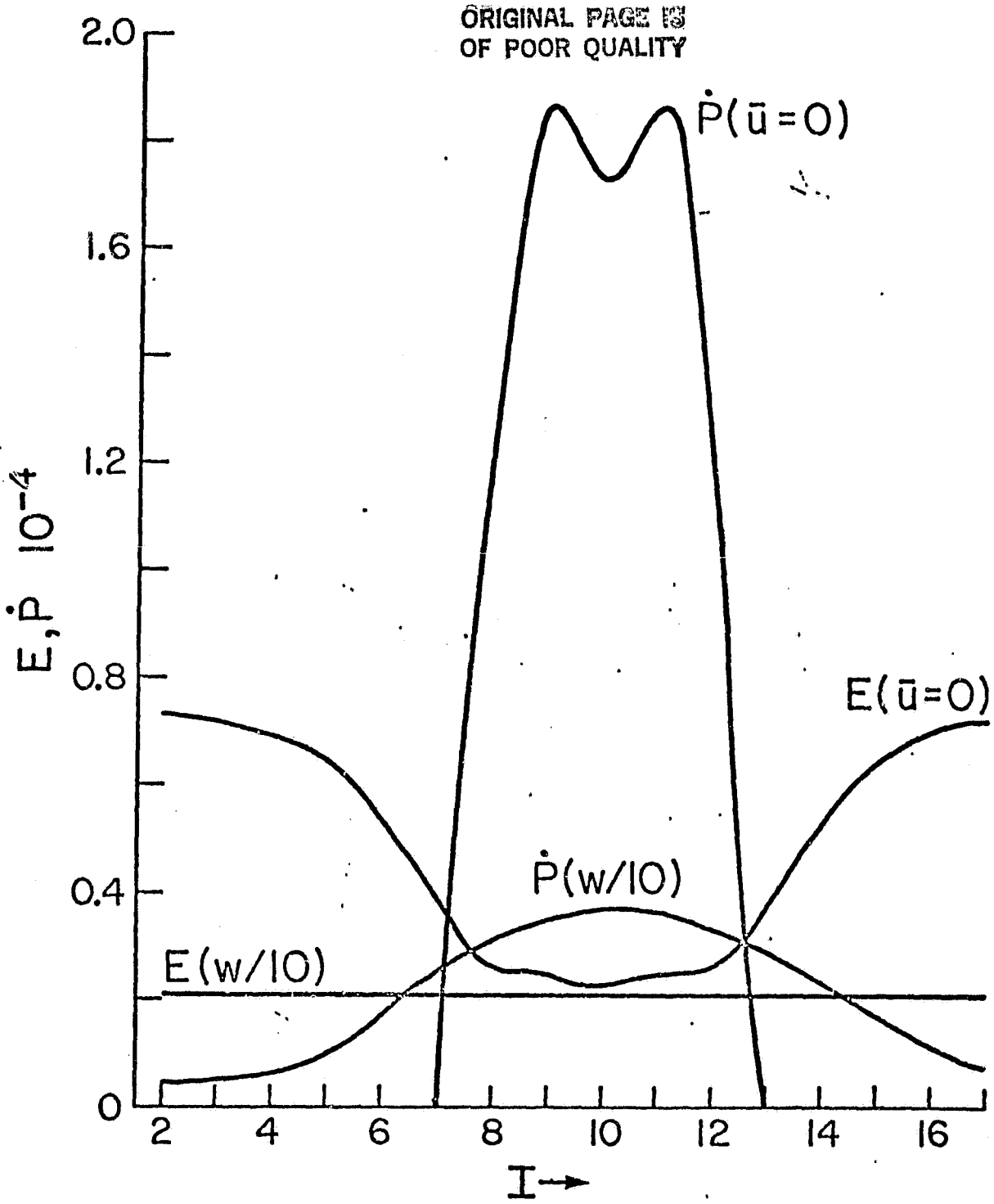

Figure 5

ORIGINAL PAGE IS
OF POOR QUALITY

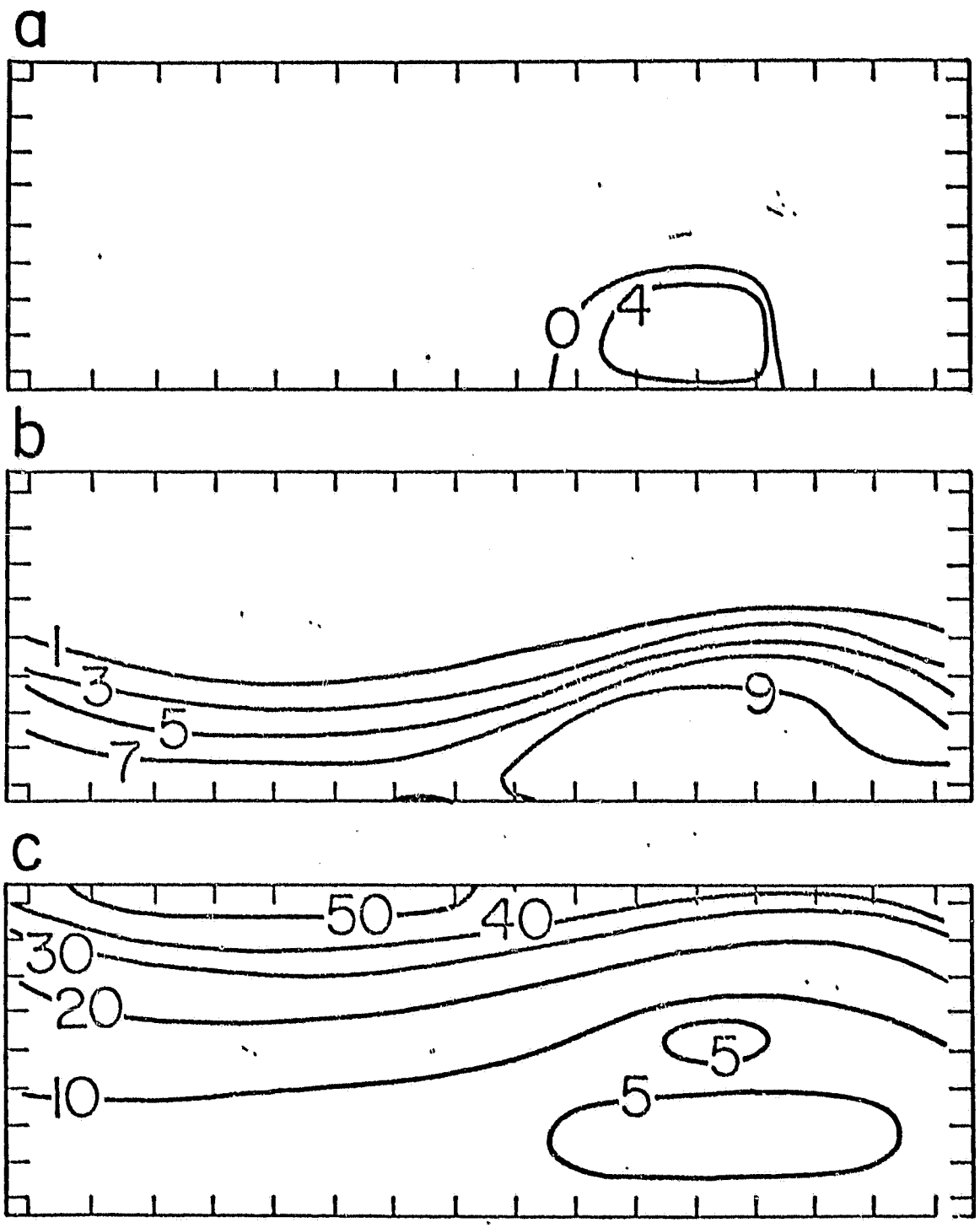

Figure 6

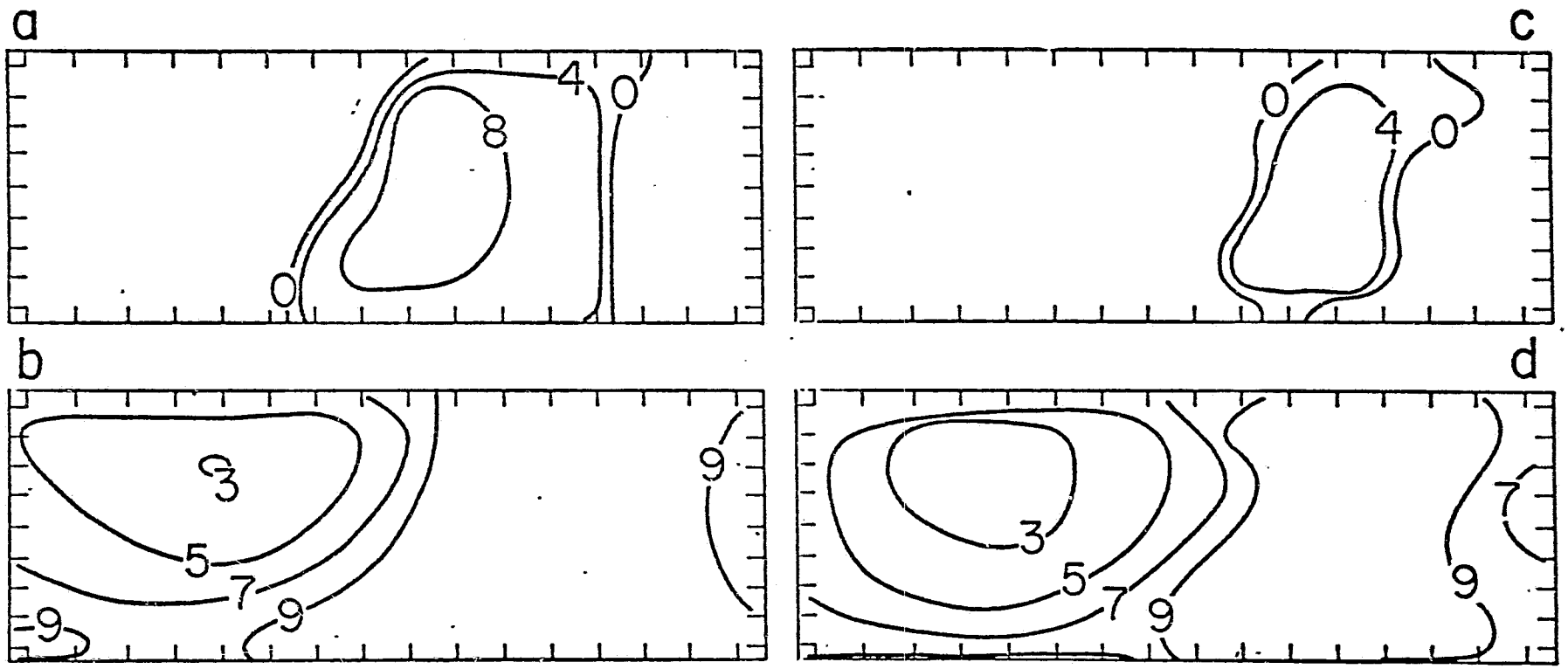

Figure 7

ORIGINAL PAGE IS
OF POOR QUALITY

ORIGINAL PAGE IS
OF POOR QUALITY

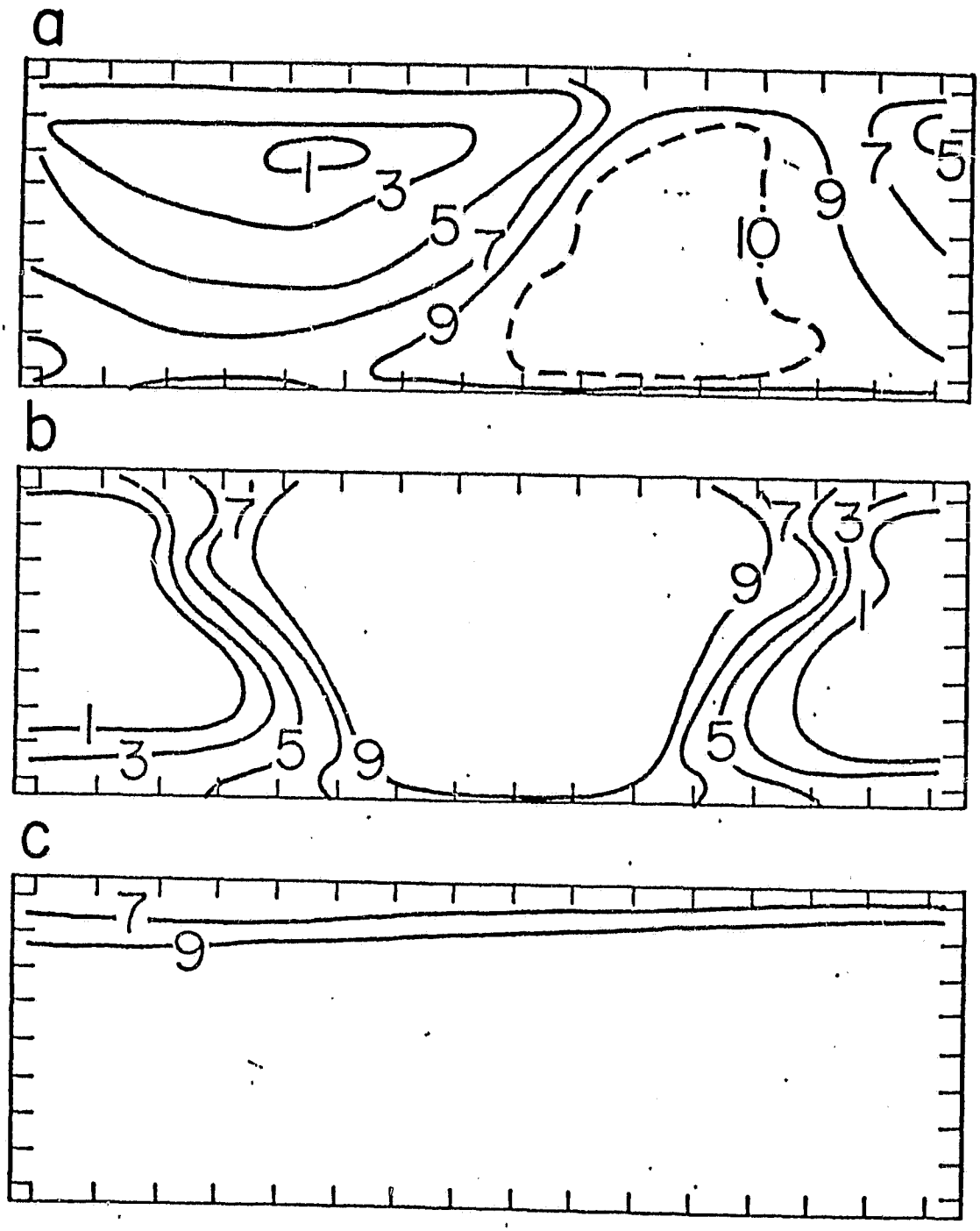

Figure 8

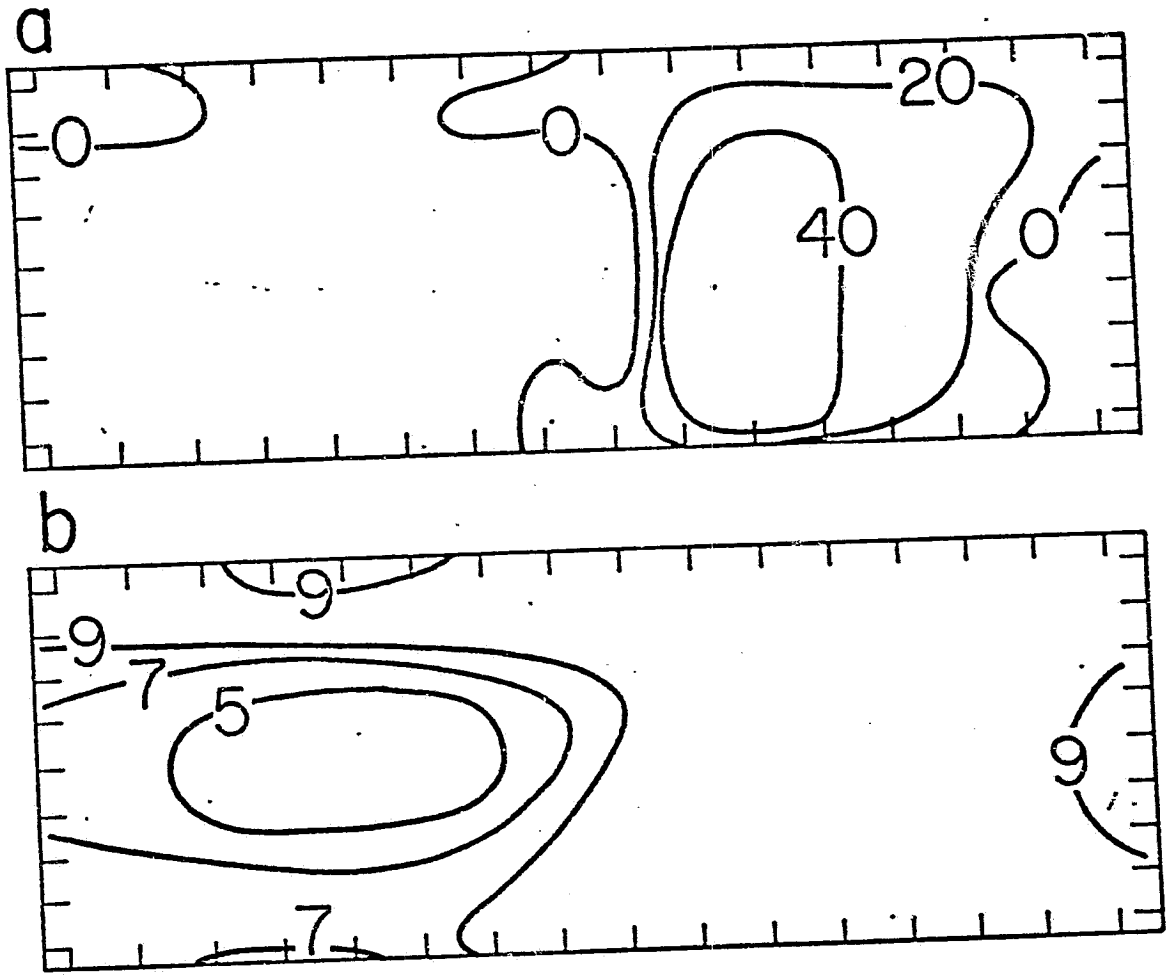

ORIGINAL PAGE IS
OF POOR QUALITY

Figure 9

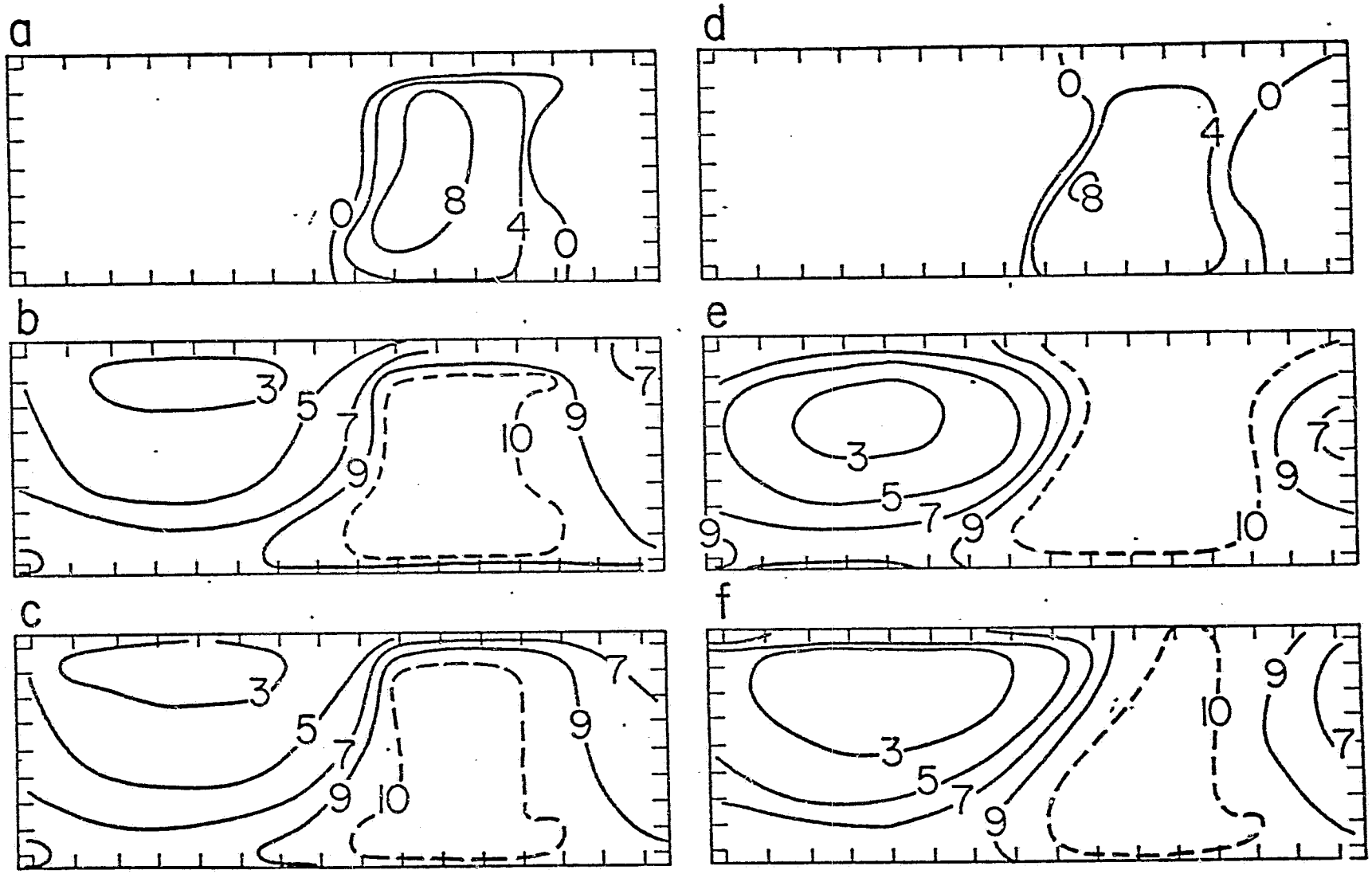

Figure 10

ORIGINAL PAGE IS
OF POOR QUALITY

ORIGINAL PAGE IS
OF POOR QUALITY

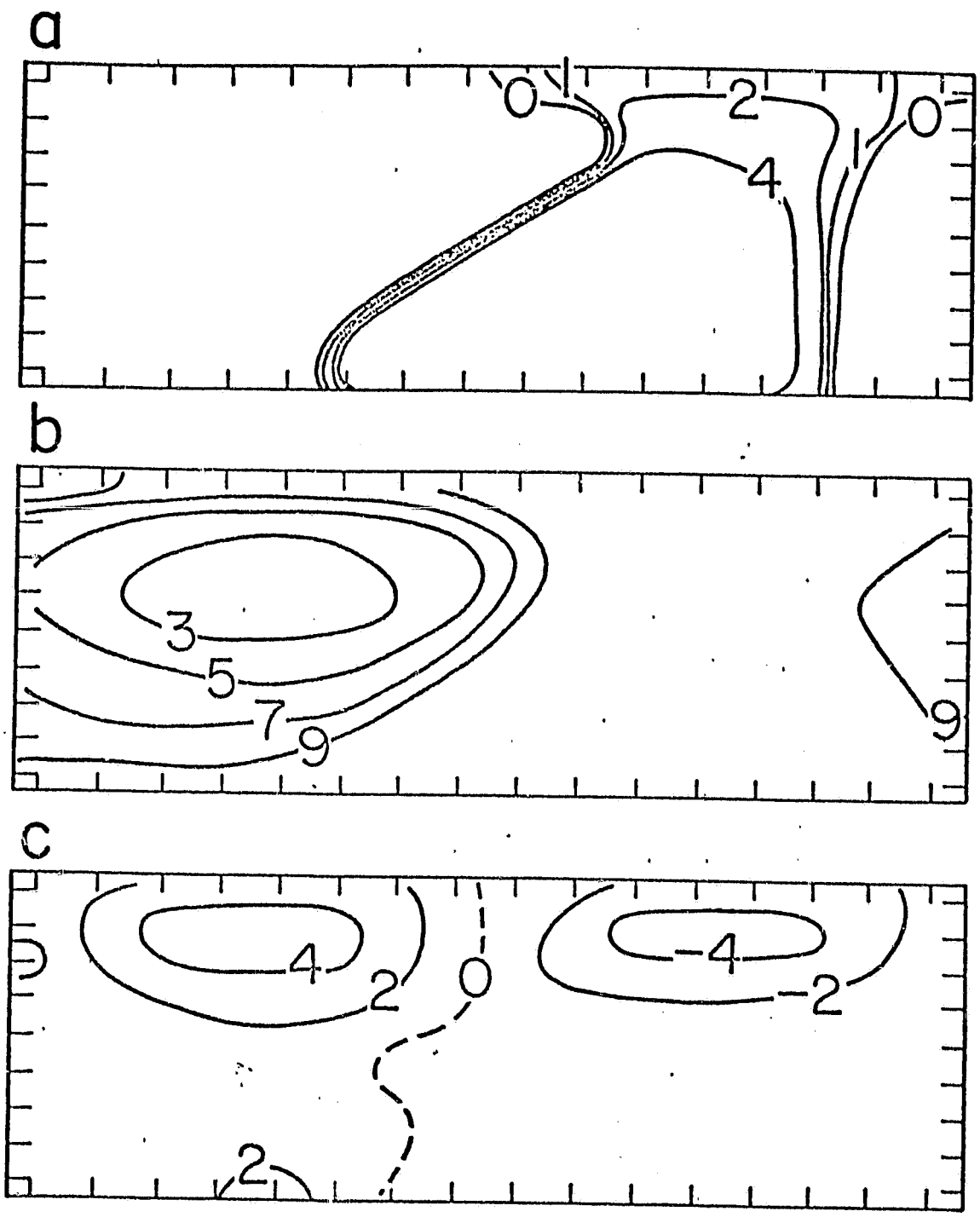

Figure 11

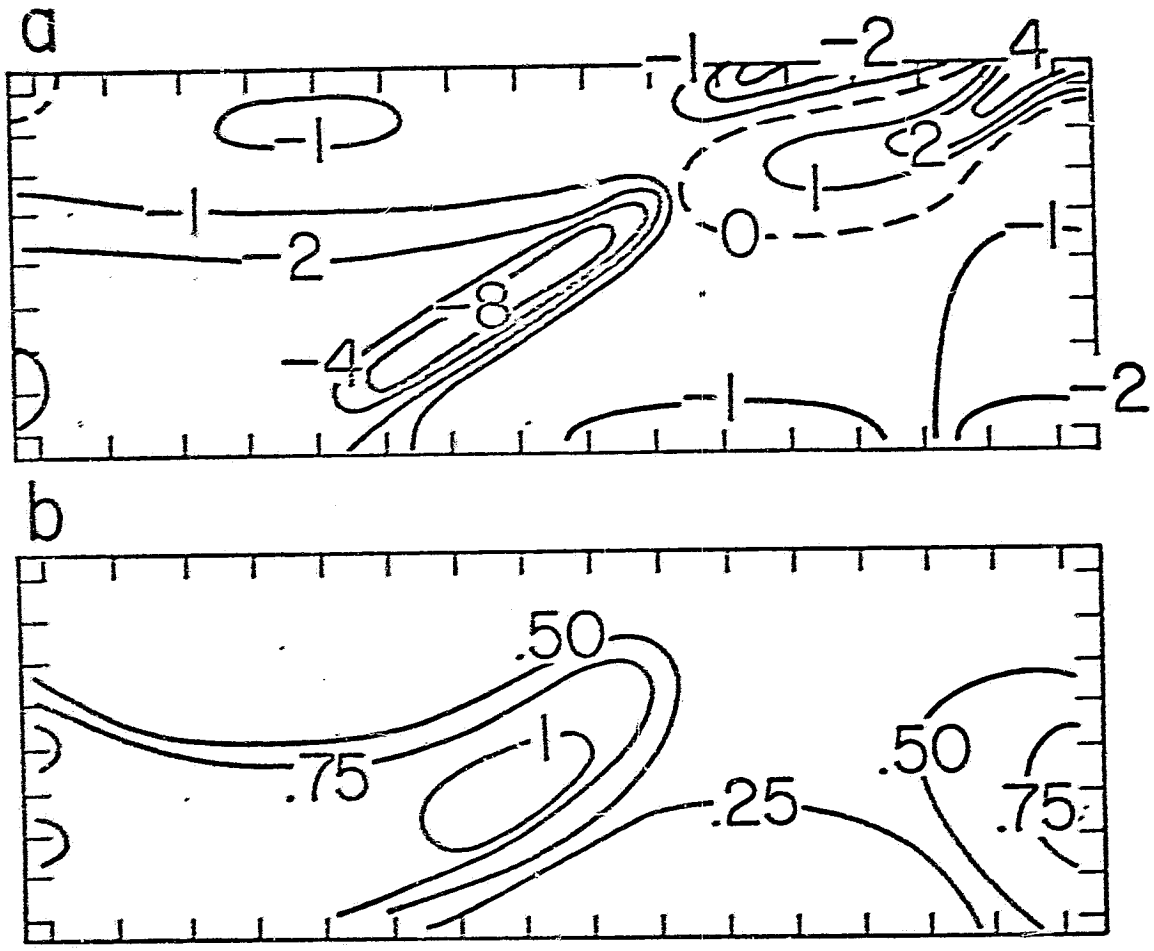

Figure 12

ORIGINAL PAGE IS
OF POOR QUALITY

ORIGINAL PAGE IS
OF POOR QUALITY

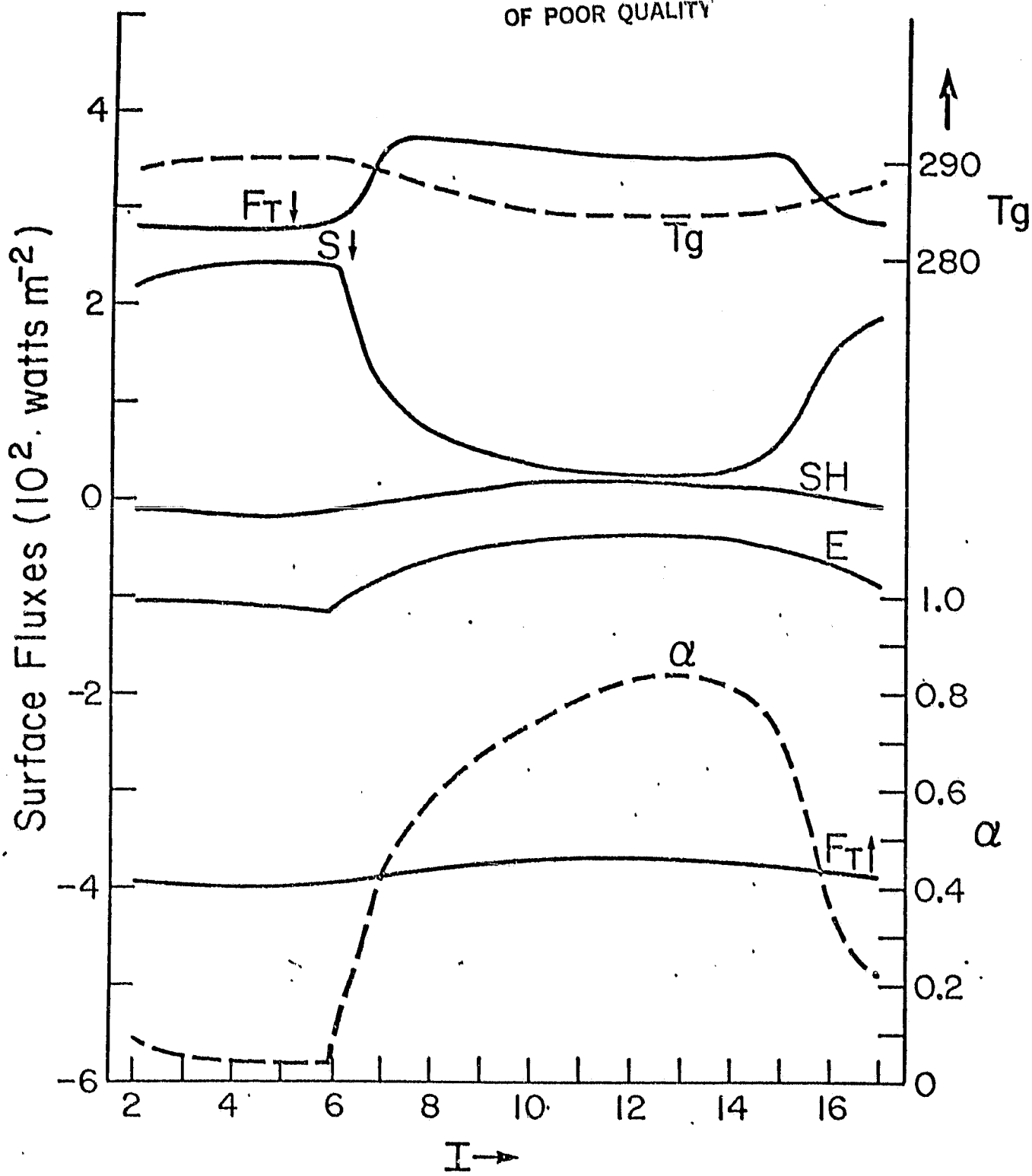

Figure 13

ORIGINAL PAGE IS
OF POOR QUALITY

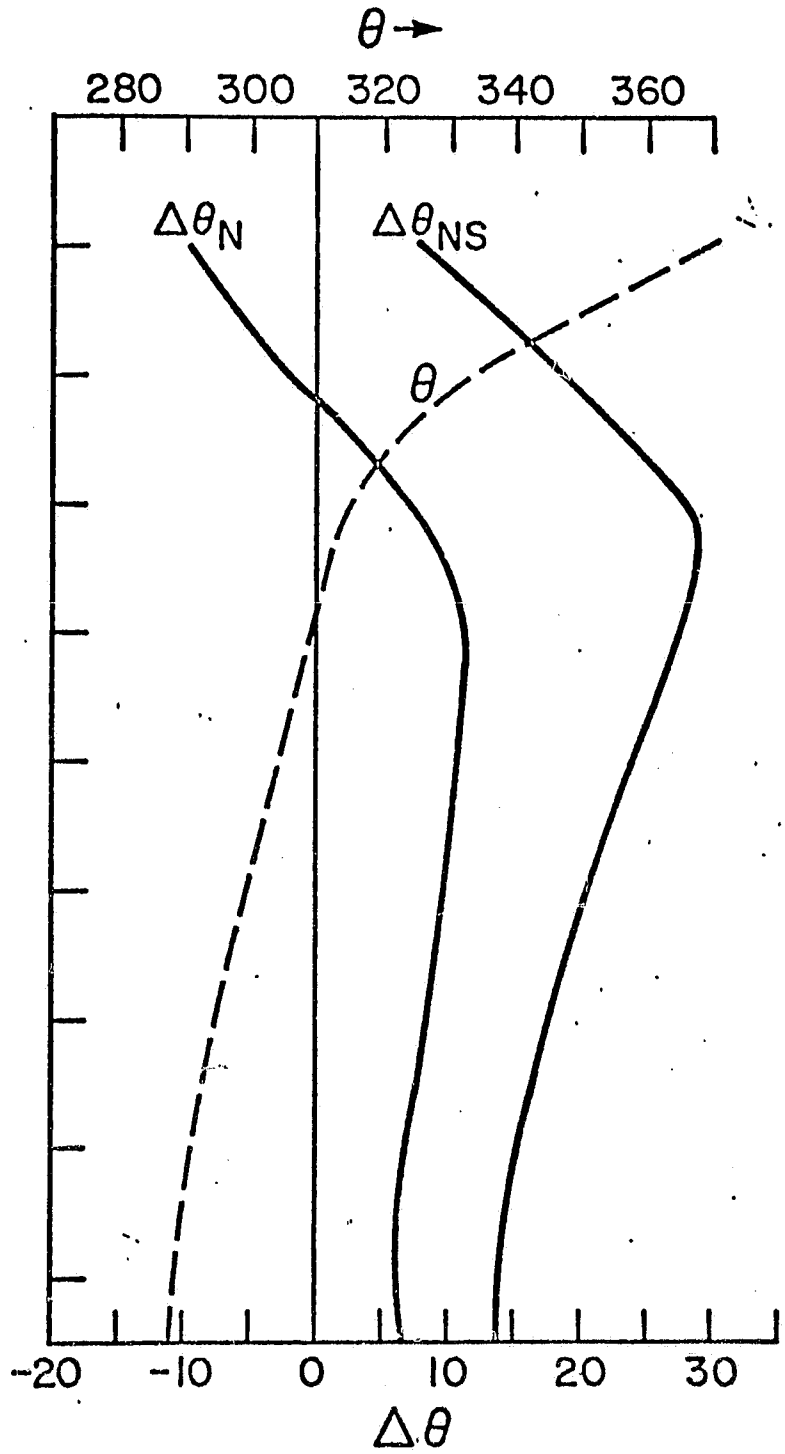

Figure 14

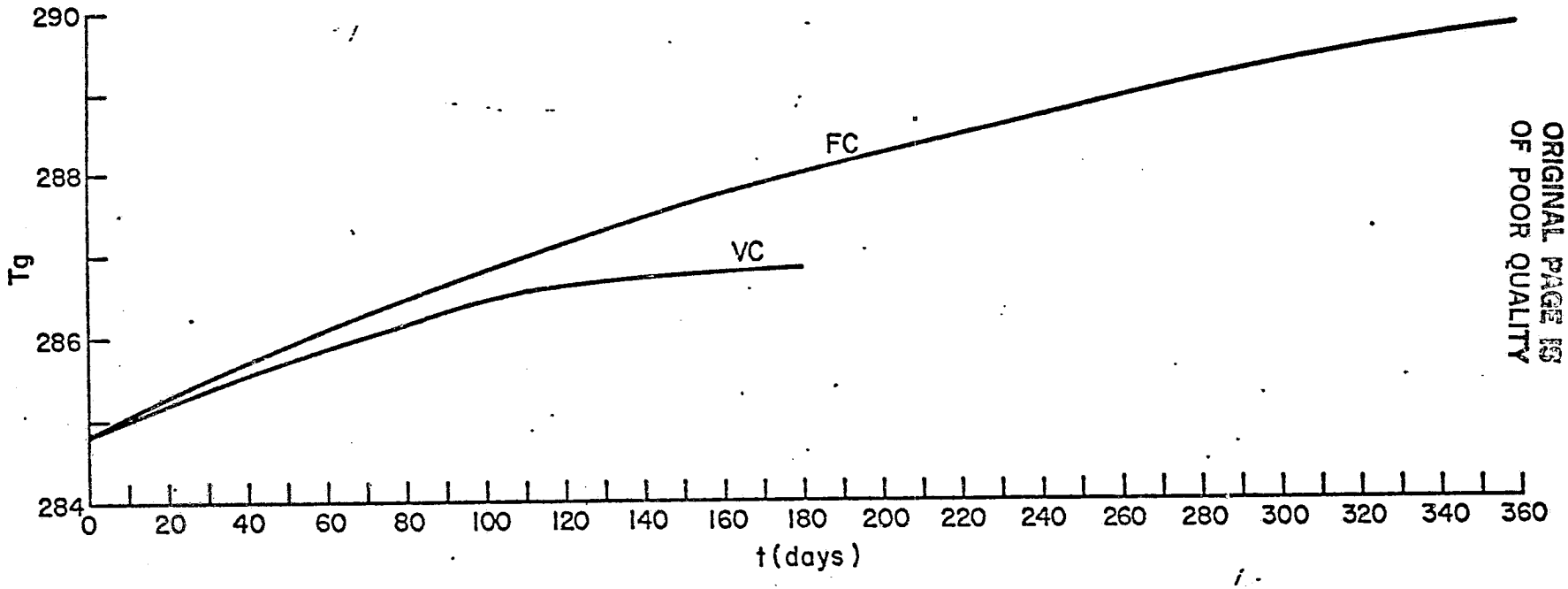

ORIGINAL PAGE IS
OF POOR QUALITY

Figure 15

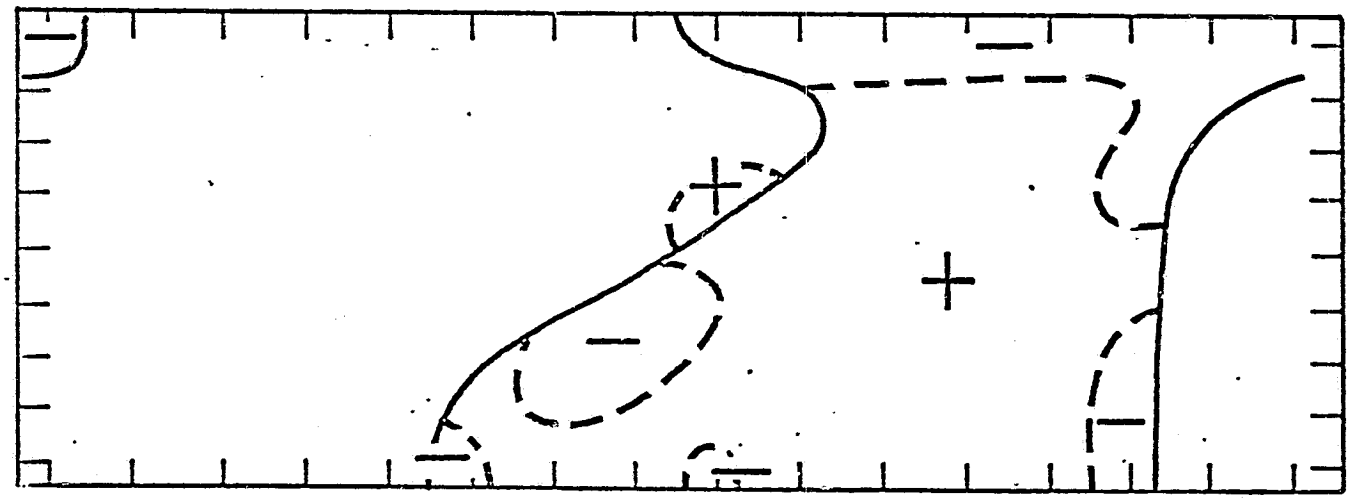

Figure 16

ORIGINAL PAGE IS
OF POOR QUALITY

ORIGINAL PAGE IS
OF POOR QUALITY

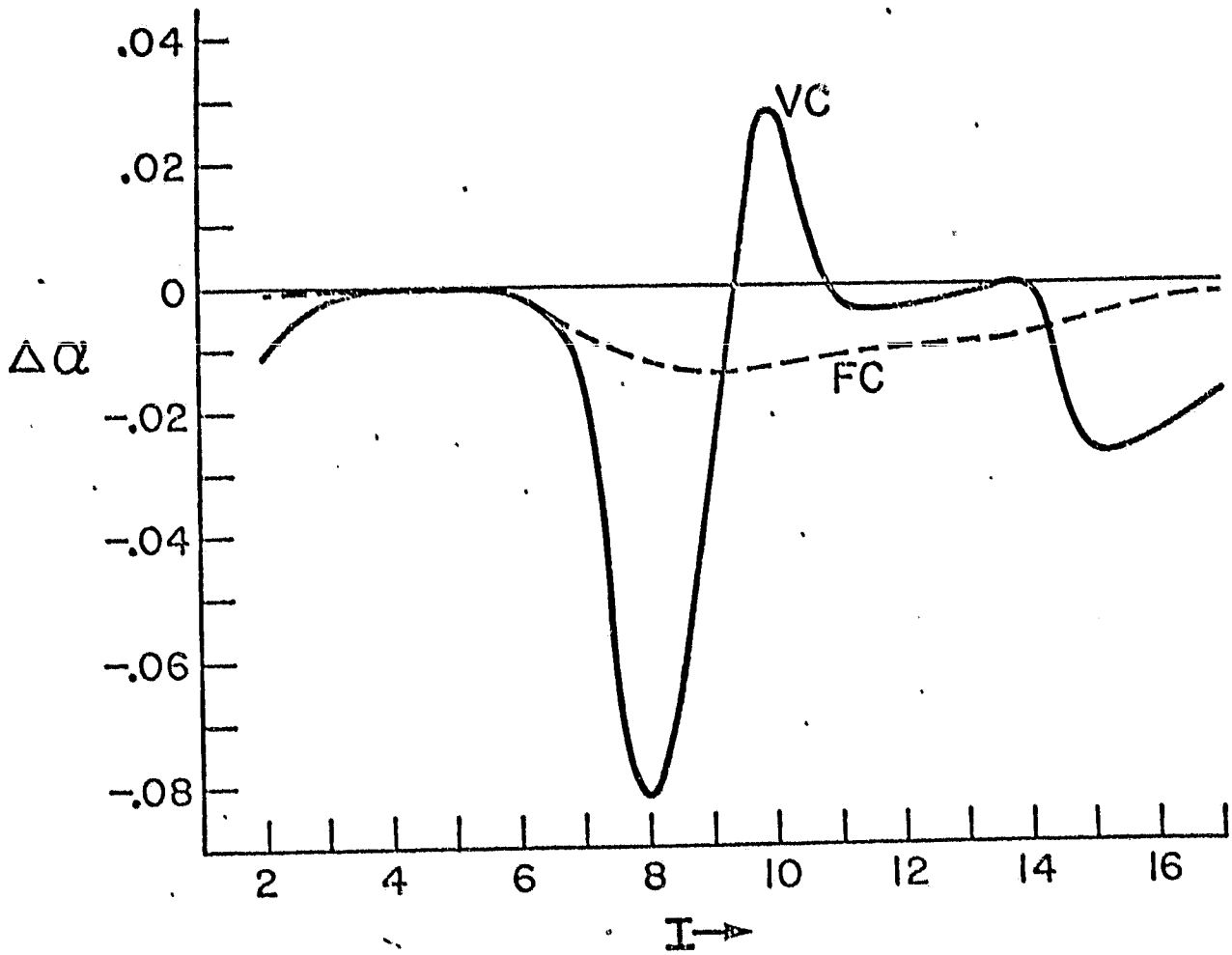

Figure 17

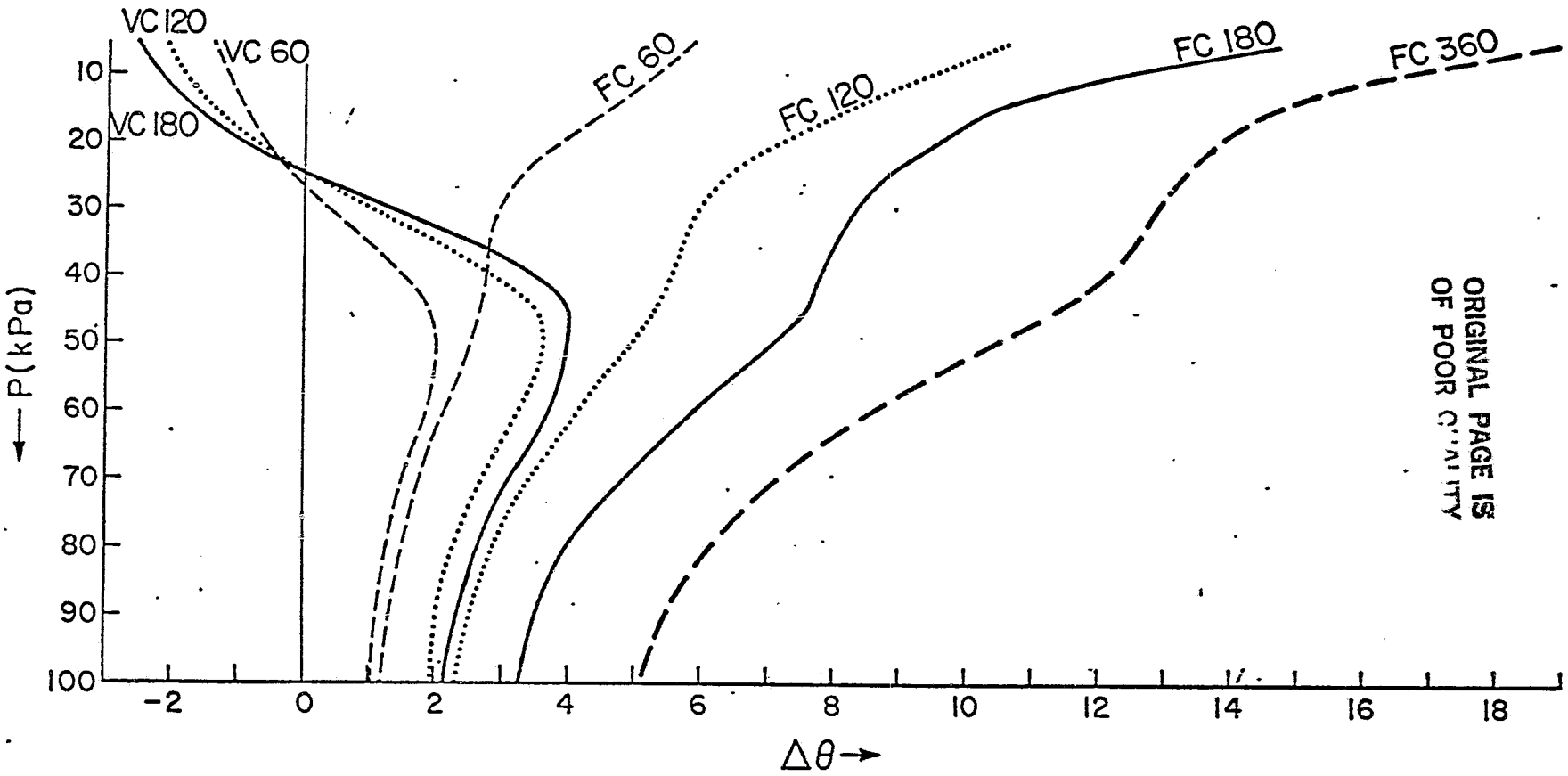

ORIGINAL PAGE IS
OF POOR QUALITY

Figure 18